

Schwann Cell Myelination Requires Integration of Laminin Activities

**Karen K. McKee^{1*}, Dong-Hua Yang^{1*}, Rajesh Patel¹, Zu-Lin Chen²,
Sidney Strickland², Junichi Takagi³, Kiyotoshi Sekiguchi⁴,
and Peter D. Yurchenco^{1†}**

¹Department of Pathology & Laboratory Medicine, Robert Wood Johnson Medical School, Piscataway, NJ 08854, ²Laboratory of Neurobiology and Genetics, Rockefeller University, New York, NY 10021, ³Laboratory of Protein Synthesis and Expression, Institute for Protein Research, Osaka University, Suita, Osaka 565-0871, Japan, ⁴Laboratory of Extracellular Matrix Biochemistry, Institute for Protein Research, Osaka University, Suita, Osaka 565-0871, Japan.

*These authors contributed equally.

†Address correspondence to: Peter D. Yurchenco, Department of Pathology and Laboratory Medicine, Robert Wood Johnson Medical School, 675 Hoes Lane, Piscataway, NJ 08854. Tel. 732-235-5166 /4674; Fax. 732-235-4825, Email. yurchenc@umdnj.edu.

Abbreviated title: Laminin-dependent myelination

Number of words in abstract: 218

Number of words in text (without bibliography): 7967

Keywords: peripheral neuropathy, muscular dystrophy, basement membrane, axonal sorting, integrin.

ABSTRACT

Laminins promote early stages of peripheral nerve myelination by assembling basement membranes (BMs) on Schwann cell surfaces, leading to activation of $\beta 1$ -integrins and other receptors. The BM composition, structural bonds and ligands needed to mediate this process, however, are not well understood. A mouse hypomorphic for laminin $\gamma 1$ -subunit expression that assembled endoneurial BMs with reduced component density exhibited an axonal sorting defect with amyelination but normal Schwann cell proliferation, the latter unlike the null. To identify the basis for this, and to dissect participating laminin interactions, *Lamc1* gene-inactivated dorsal root ganglia were treated with recombinant laminins-211 and -111 lacking different architecture-forming and receptor-binding activities to induce myelination. Myelin-wrapping of axons by Schwann cells was found to require higher laminin concentrations than either proliferation or axonal ensheathment. Laminins that were unable to polymerize through deletions that removed critical LN-domains, or that lacked cell-adhesive LG-domains, caused reduced BMs and nearly absent myelination. Laminins engineered to bind weakly to $\alpha 6\beta 1$ and/or $\alpha 7\beta 1$ integrins through their LG-domains, even though they could effectively assemble BMs, decreased myelination. Proliferation depended upon both integrin-binding to LG domains and polymerization. Collectively these findings reveal that laminins integrate scaffold-forming and cell-adhesion activities to assemble an endoneurial BM, with myelination and proliferation requiring additional $\alpha 6\beta 1/\alpha 7\beta 1$ -laminin LG-domain interactions, and that a high BM ligand/structural-density is needed for efficient myelination.

INTRODUCTION

In peripheral nerve, basement membranes (BMs) play a critical role in the maturation of Schwann cells by promoting radial axonal sorting leading to myelination (Bunge et al., 1986; Webster, 1971; Webster et al., 1973). The process is dependent upon $\beta 1$ -integrins that bind to BM ligands to mediate sorting and Schwann cell proliferation (Benninger et al., 2007; Berti et al., 2011; Nodari et al., 2007; Pereira et al., 2009). BMs also bind to α -dystroglycan and $\alpha 6\beta 4$ integrin; however, these mediate later stages of myelination, affecting nodal development and myelin-sheath stabilization (Berti et al., 2011; Nodari et al., 2008; Saito et al., 2003). Finally BMs may tether heparin-binding growth-factors such as soluble neuregulin (Ma et al., 2011). Despite this information, little is actually known about the critical receptor ligands and structural contributions of BMs that are required for the progression of stages leading to myelination.

Laminins are a family of glycoproteins that along with nidogens, type IV collagen and the proteoglycans perlecan and agrin constitute the major components of BMs. Laminins are required to initiate BM assembly (Smyth et al., 1999). Assembly depends upon laminin adhesion to cell surfaces, polymerization, and binding to nidogens and agrin (Li et al., 2005; McKee et al., 2007; Yurchenco, 2011). Laminins also mediate BM-dependent functions by interacting with integrins and dystroglycan (reviewed in Li et al., 2002). The laminin requirement poses a challenge for dissecting BM contributions given the complexity of ligands within BMs and the relative inability to distinguish laminin from non-laminin contributions.

Schwann cell laminins share the $\gamma 1$ -subunit in the principal endoneurial laminin-211 (Lm211, $\alpha 2\beta 1\gamma 1$ subunit composition) and the minor laminins 411 and 511. Inactivation of *Lamc1*-gene expression or combined inactivation of the *Lama2* and *Lama4* genes each caused a severe peripheral neuropathy characterized by amyelination and reduced proliferation (Chen and Strickland, 2003; Yu et al., 2005; Yang et al., 2005). Inactivation of the $\beta 1$ -integrin gene in Schwann cells caused substantial peripheral nerve disease, particularly severe in a C57Bl6 background, similar to the *Lamc1* Schwann cell knockout phenotype (Berti et al., 2011).

We now describe a mouse with intermediate-level laminin $\gamma 1$ subunit expression with an axonal sorting defect not accompanied by reduced Schwann cell proliferation, the latter attribute distinct from the *Lamc1* laminin knockout and other laminin deficiency states. This defect was characterized by hypomyelination, alterations of SC myelination factors, and accompanied by muscle atrophy and dystrophy. Investigation of the role of laminins and their functional domains in cultured dorsal root ganglia (DRG) rendered incompetent to secrete $\gamma 1$ -laminins revealed that laminin cell surface anchorage and polymerization are important for BM assembly and that laminin concentration, polymerization, and $\beta 1$ -integrin interactions differentially contribute to promote proliferation, ensheathment and myelination.

RESULTS

Laminin hypomorphic mice: *Lamc1*^{fl^{neo}/-} mice were undistinguishable from their fl^{neo}/+ littermates until three weeks of age. When lifted by tail, the fl^{neo}/+ mice extended their hindlimbs outwards. In contrast, hindlimbs of fl^{neo}/- mice were slightly tremulous and retracted inwards. By 8-10 weeks of age, the affected mice exhibited sustained hindlimb contractures and reductions of muscle mass in the lower back and hindlimbs with difficulty in ambulation. The possibility that the gait abnormality might be due to the presence of the *neo* selection cassette was supported by the finding fl/- offspring lacking the cassette did not develop a gait abnormality and appeared normal in their behavior throughout life.

Morphology of adult peripheral nerve: Sciatic nerves and other tissues were dissected from fl^{neo}/- mice and their fl^{neo}/+ littermates (10 to 24 weeks) and examined by microscopy (**Fig. 1** and supplemental **Fig. S1**). Methylene blue-stained semi-thin sections of sciatic nerve and nerve roots of fl^{neo}/- mice exhibited multiple pale-staining areas corresponding to amyelinated axons compared to littermate controls (Fig.1,A-D). Larger amyelinated areas were found in the fl^{neo}/- nerve roots (Fig.1C,F). The ultrastructure of the sciatic nerves was examined in adults (Fig. 1 G, H). Compared to littermate controls, fl^{neo}/- nerves had a two-fold reduction of myelinated axons and near-complete absence of enveloped axons (Remak bundles) with many naked axons (Fig. 1 and supplemental **Fig. S2A**). This was accompanied by a seven-fold increase in SCs that do not myelinate, mostly located adjacent to naked axons. *Lamc1* fl^{neo}/- nerves were hypomyelinated with increased axon/myelin+axon ratios. The thickness of adult SC BMs was found to be the same.

Post-natal nerve: Sciatic nerve ultrastructure was also examined at post-natal day 5 (P5) during the stage of active axonal-sorting (supplemental **Fig. S3**). SC lamellipodial processes (LP) were noted to extend into and divide bundles of axons, and to envelop axons and axon groups, in both *Lamc1*^{fl^{neo}/+} and fl^{neo}/– sciatic nerve. Longer processes extending from SC bodies were often seen to encompass groups of axons in which the BM was always located on the opposite side as the axons (lower panel), reflecting a polarity of structure. Scattered myelinated axons were present as well. However, the naked axon bundles were larger in mutant nerve with less extensive penetration and separation by SC processes. SC BMs possessed frequent discontinuities along the LP surfaces and portions of SC bodies in the fl^{neo}/– nerves in contrast to fl^{neo}/+ nerves. The BMs of myelinated axons (MA), on the other hand, were essentially continuous in control and mutant nerves. Length measurements of LP BMs relative to the underlying plasma membranes revealed a two-fold decrease of BM.

Laminin mRNA: The nerve and muscle phenotype suggested a laminin deficiency state. RNA extracts from the nerve, muscle, and other organs were measured by quantitative real-time RT-PCR (**Fig.2A** and Fig.S1,A,B). There was a reduction of laminin- γ 1 mRNA isolated from fl^{neo}/– mice compared to that of +/+ mice (36% average relative to wild-type), implicating the floxed-allele paired with a null-allele as the basis of reduced laminin expression. Since a lesser degree of reduction of mRNA was observed for mRNA isolated from *Lamc1*+/- mice (average of 67%) that have no evidence of disease, it suggests that the threshold for development of a phenotype from a *Lamc1*mRNA exists between 36 and 67% of wild-type. Somewhat surprisingly, the decrease in mRNA from fl^{neo}/ fl^{neo} relative to +/+ mice was almost negligible, suggesting an enhancement of mRNA expression may result from an interaction between the two identical alleles

not present in $fl^{neo}/-$. Removal of the neo cassette from the floxed allele alone was sufficient to restore mRNA expression to levels approaching those of the wild-type (+/+) state (Fig.S1,A), implicating the presence of the neo cassette *cis* to the active allele as the cause of reduced expression. This is in keeping with published reports that the *neo* cassette (including that of the *Lama5* gene) can be a cause of reduced neighboring gene expression (Meyers et al., 1998; Shannon et al., 2006). The mRNA level for laminin $\beta 1$, $\gamma 3$, $\alpha 2$, and $\alpha 4$ (nerve, muscle), and $\alpha 5$ (kidney and lung) was found not to be different for $fl^{neo}/+$ and $fl^{neo}/-$ littermates (Fig.S1B).

Basement membrane protein in peripheral nerve and other tissues. Immunostaining of adult sciatic nerve revealed similar BM-pattern reductions of laminin subunits $\gamma 1$, $\beta 1$, $\alpha 2$, $\alpha 4$, $\gamma 3$ (slight), collagen-IV and perlecan (Fig. 2B). Integrin subunits $\alpha 6$ and $\beta 1$ and dystroglycan changed little if at all. Since the adult BM structural components in nerve were less bright by immunostaining without recognizable changes in ultrastructure, it was concluded that the endoneurial BMs possessed a lower density of these components. The reduction in these laminin-associated components is predicted given formation of a BM is dependent upon laminin expression (Li et al., 2002; Li et al., 2005; McKee et al., 2007). Reductions of BM components, but not integrin or dystroglycan, were noted for hindlimb muscle (quadriceps); however, these reductions were not as great as those noted in peripheral nerve (Fig. S1,C). Slight reductions of *Lmy1* were noted in lung and kidney glomeruli with no reductions appreciated in colon (Fig. S1D-E). Hindlimb nerve at E18.5, P1 and P5 revealed differences similar to those in adults (supplemental **Fig. S4**). The relative lack of laminin reductions in non-neuromuscular tissues, despite comparable reduced *Lmy1* mRNA, might be due either to a higher transcriptional efficiency or to high levels of $\gamma 1$ subunit production relative to the other subunits. The latter possibility is deduced

from the finding that secretion of laminins is limited by the subunit synthesized in least amount (Yurchenco et al., 1997).

Schwann cell proliferation and myelination factor expression: While there is diminished SC proliferation in the conditional SC *Lamc1* gene knockout (Yu et al., 2005), reduced SC proliferation was not detected in hypomorphic nerve in nerve, even at the time of peak proliferation that occurs just before and at the time of birth (**Fig. 3,A,B** with plots in G,I). The mRNA levels for SC-factors involved in myelination were determined by quantitative RT-PCR in adult and P5 sciatic nerve (**Fig. 3,C,D**). Elevations of the transcription factors cJun, Oct6 and Sox2 and reductions of Krox20, the p75 neuregulin receptor, and myelin-protein-zero (MPZ) were detected in mutant nerve.

Muscular atrophy and dystrophy: Hindlimb muscle mass was observed to gradually become reduced in *Lmy1 fl^{neo}/-* mice. The quadriceps were abnormal in that they were populated by scattered small myotubes and central nuclei in the absence of obvious endomysial fibrosis at the light microscopic level, although a slight but distinct increase in interstitial collagen fibrils was appreciated by ultrastructure (supplemental **Fig. S5**). The sarcolemmal BMs appeared normal. Quantitation of the muscle diameter revealed significantly smaller muscle diameter (atrophy) in *fl^{neo}/-* mice.

Induction of myelination in dorsal root ganglion cultures with recombinant laminins: In order to better understand mechanisms underlying the nerve phenotype resulting from reduced and absent

laminin expression, an analysis using laminin-deficient cultured dorsal root ganglia cultures treated with wild-type and modified recombinant laminins was conducted.

Laminin cell-adhesion (e.g. sulfatides), integrin-binding, dystroglycan-binding, polymerization, and nidogen-binding activities map to different structural domains and have been selectively inactivated through engineered deletions or point-mutations (**Fig. 4**) allowing for loss-of-function analysis (McKee et al., 2009; McKee et al., 2007; Smirnov et al., 2002). In addition, laminin-binding linker proteins that fuse laminin-domains to nidogen-domains and modified agrin allow for gain-of-function analysis (McKee et al., 2009). The C-terminal Flag-tag, present in two of the laminins, consists of eight nearly all charged amino acid residues that are located four residues downstream of a glutamic acid required for integrin interactions with laminin LG domains and that similarly impede integrin-binding (Ido et al., 2007).

Previous studies of SCs cultured with sensory neurons of rat dorsal root ganglia (DRG) have shown a role of BMs in myelination (Ard et al., 1987; Clark and Bunge, 1989; Eldridge et al., 1989). The presence of endogenous laminin production and baseline myelination by SCs limits this approach for further dissection of laminin contributions to myelination, particularly when BM assembly is induced with ascorbate (Eldridge et al., 1989; Eldridge et al., 1987). It was found that this limitation can be overcome with DRGs isolated from conditional knock-out mice treated with adeno-cre-recombinase virus to prevent expression of the laminin- γ 1 subunit common to Lm211, Lm411 and Lm511 (Paivalainen et al., 2008; Yu et al., 2009), and in which BM assembly, ensheathment and myelination are then initiated by the addition of exogenous laminin to the culture medium. To analyze the contributions of laminin concentration and laminin-

domain activities to these processes, the laminin-deficient DRGs were treated with recombinant laminins that are wild-type or that possess structural modifications and that have been characterized by rotary shadowing, self-assembly, binding-interactions and BM assembly on isolated Schwann cells (McKee et al., 2009; McKee et al., 2007, Smirnov et al., 2002, and data not shown). While Lm211 is the principal laminin of peripheral nerve, Lm111 has been found to restore myelination in nerve following transgenic expression of the Lm α 1 subunit in Lm α 2^{-/-} (dy3K) mice, indicating the laminin possesses the necessary domains for proper function (Gawlik et al., 2006). The evaluation was largely conducted with Lm111 and supported with Lm211 comparisons.

The cultured DRG explants consist of neuronal cell bodies concentrated in the central region that extend out axonal-like processes with SCs resting on and between these processes, and with only a few scattered fibroblasts detected. In the absence of added laminin, very little if any laminin was detected by immunostaining with antibody to Lm α 2 (the principal α -subunit) from the time of virus infection to six days after addition of ascorbate (supplemental **Fig. S6,A**). Pilot experiments with added Lm111 revealed that peak proliferation occurred about the time of addition of ascorbate and that myelination developed after ascorbate addition (data not shown). The ascorbate induction is a consequence of increased secretion of stable type IV collagen that presumably also induces laminin (Eldridge et al., 1987). Various laminins along with recombinant nidogen-1 (28 nM, to promote binding to type IV collagen) were added to the medium of the DRGs starting at the time of viral addition and extending through the switch to ascorbate-containing medium to induce myelination. Proliferation (estimated by the segmented ratio of EdU incorporated into nuclei undergoing DNA synthesis to Dapi-stained nuclei) occurred at low levels in the

absence of laminin and increased with added rLm111; however, a plateau was approached above 3.5 nM (**Fig. 5**,A-E,K, L). In contrast, myelination (measured by the segmented ratio of MBP/NFL+gfp, or by total myelinated segment lengths/DRG area) was found to increase with increasing concentrations of exogenous rLm111 over the range examined (Fig.5, F-J,K,M and Fig. S6,B).

Schwann cell adhesion and integrin-binding: The cell adhesion attributes of DRG-derived SCs with respect to laminins and other BM components were examined with SCs isolated from DRG cultures (**Fig. 6**). SCs adhered to, and spread on rLm111 and collagen-IV. Additional weaker adhesion and spreading were observed for miniagrin (which contains the cell-adhesive LG domains), and only poor adhesion was observed with nidogen-1. rLm111 lacking the first three LG domains (rLm $\Delta\alpha$ 1LG1-3) required for integrin-binding (Nishiuchi et al., 2006) did not support adhesion at all. rLm211 also supported SC adhesion and spreading; however, a higher coat concentration was required compared to rLm111 (Fig. 6B). rLm111 or rLm211 bearing a Lmy1-Flag-tag exhibited reduced cell adhesion compared to their normal counterparts. Binding of soluble integrins to rLm111 and rLm211 revealed that α 7X2 β 1 was substantially reduced when either laminin possesses a C-terminal Flag-tag and that, in the case of rLm111, Flag-tag conferred weaker binding to integrin α 6 β 1. Furthermore, α 3 β 1 was found to be the integrin that binds miniagrin.

The ability of these recombinant laminins to induce myelination and form a BM was examined in the virus-induced laminin-deficient DRGs (**Fig. 7**). Myelination was found to be extensive following treatment with 28 nM wild-type rLm111 and, to a somewhat lesser degree,

with rLm211. However, myelination was considerably reduced when DRGs were incubated with Flag-tagged rLm111F and rLm211F that were found to bind poorly to β 1-integrins that normally bind to laminin LG domains. Deletion of the proximal three LG domains of rLm111 (rLm $\Delta\alpha$ 1LG1-3), essential for integrin-binding to laminin LG domains and also containing an LG2 sulfated-glucuronate binding activity, prevented myelination. Incubation of DRGs with rLm $\Delta\alpha$ 1LG1-3 coupled to miniagrin (binds strongly to the laminin coiled-coil and interacts with cell surfaces through sulfatides, dystroglycan and α 3 β 1 integrin) generated a slight degree of myelination. Myelination was nearly completely absent when DRGs were treated with rLm111 bearing a deletion of the distal LG4-5 domains that mediates dystroglycan-, sulfatide- and heparin-binding (Harrison et al., 2007).

Myelination was nearly absent following treatment of DRGs with rLm $\Delta\alpha$ 1LN-L4b, a laminin unable to polymerize and that lacks a secondary potential locus of cell-interaction (α 1LN domain binds to sulfatides, α 1 β 1/ α 2 β 1, and heparin; Colognato-Pyke et al., 1995; McKee et al., 2009; McKee et al., 2007). Given that earlier studies with SCs revealed a sulfatide-, but not a heparan sulfate-dependency of BM assembly (Li et al., 2005), and our inability to detect a contribution to SC adhesion in the absence of LG domains, it was presumed that the critical lost activities in rLm $\Delta\alpha$ LN-L4b were polymerization and possibly sulfatide-binding. However, a comparable reduction of myelination was observed with rLm $\Delta\beta$ 1LN-LEa, whose deleted domains are associated only with polymerization (McKee et al., 2009; McKee et al., 2007), confirming that ablation of polymerization alone is sufficient on its own to prevent myelination. Furthermore, evidence for a key polymerization role was provided by the observation that myelination could be significantly restored by binding α LNNd, a fusion protein that binds to the nidogen-

binding locus and provides the critically missing α 1LN domain to rLm $\Delta\alpha$ 1LN-L4b (but not to rLm $\Delta\beta$ 1LN-LEa that lacks the β 1LN rather than the α 1LN domain)(McKee et al., 2009). Finally, it was found that DRG myelination was reduced, albeit slightly, with a laminin (rLm111NS) unable to bind to nidogen.

Addition of rLm111 to the DRGs led to increased accumulation of laminin subunits (exogenous) as well as endogenously-derived Schwann cell type IV collagen and perlecan (Fig. 7,C). Thus it appears that multi-component BMs, and not just laminin ECMs, had assembled. Finally, comparisons of rLm211F to rLm211F and rLm $\Delta\alpha$ LN-L4b to rLm111 revealed that presence of the integrin-reducing modification results in a decrease in proliferation while absence of polymerization reduces laminin-induction of proliferation to baseline (laminin-free) levels (Fig. 7,D).

DRG ultrastructure: DRGs treated with laminins was examined by electron microscopy (**Fig. 8**, Fig. S6,E-I). In the absence of added laminin, the SC lacked BMs on their surfaces. Axons were adjacent to SCs but were naked in their appearance, either adjacent to SC plasma membranes or near them. At the lowest concentration of added rLm111 (3.5 nM), substantial but incomplete BM coverage on SCs was noted characterized by BM discontinuities of variable lengths. Near-complete BM coverage were noted for the two wild-type laminins at 28 nM. The extent of BMs coverage of SCs was found to increase as a function of rLm111 concentration. A plateau was reached by 7 nM and corresponds to the peak of proliferation. Treatment with rLm111F or rLm211F did not reduce BM. In contrast, deletion of the distal LG1-3 domains, and especially deletion of the LG1-3 domains, resulted in decreased BM. These decreases might be attributed to reduction of cell-surface sulfatide-binding (LG4), dystroglycan-binding (LG4), integrin-binding

(LG1-3) and/or sulfated-glucuronate (LG2) (Hall et al., 1995; Harrison et al., 2007; Nishiuchi et al., 2006; Sung et al., 1993). However, since reduction of LG-integrin binding or dystroglycan has not been found to affect BM assembly in other studies, reduction of sulfatide-binding activity in LG4 and loss of sulfated-glucuronyl binding activity in LG2 may account for BM reductions for LG4-5 and LG1-3 deletions (Feltri et al., 2002; Li et al., 2002; Saito et al., 2003). BM was restored with miniagrin with only a partial restoration of myelination.

Laminins lacking short-arm segments ($Lm\Delta\alpha 1LN-L4b$, $Lm\Delta\beta 1LN-LEa$) with $\alpha 1LN$ and $\beta 1LN$ polymerization domains reduced BM cell coverage. BM was increased (but not to normal levels) when $\alpha LNNd$ was added to $Lm\Delta\alpha 1LN-L4b$, but not to $Lm\Delta\beta 1LN-LEa$. Previous analysis with modified rLm111 has shown that an absence of LN domains causes a failure of polymerization and BM assembly and that the polymer requires an αLN , a βLN and a γLN domain (McKee et al., 2009; McKee et al., 2007). Thus $\alpha LNNd$ provides the missing αLN domain to $Lm\Delta\alpha 1LN-L4b$ to enable polymerization, but fails to provide the $\beta 1LN$ domain missing in $Lm\Delta\beta 1LN-LEa$. Finally, laminin bearing a point mutation ($Lm\gamma 1N802S$) that ablates nidogen-1 binding resulted in BMs with only slight reduction of coverage. This suggests that nidogen-mediation of high affinity bridging of laminin to type IV collagen is less critical than polymerization for maintaining a functional endoneurial BM (Fox et al., 1991).

Axonal ensheathment was also examined (Supplemental Fig. S6, E-I) with respect to the degree of bundling and segmentation within Schwann cells to gauge the degree of axonal sorting (see Webster, 1993) for absent laminin, low and high rLm111, rLm211F, laminin-111 without LG4-5, and non-polymerizing laminin. The axons of DRGs not treated with laminin were nearly

all naked (some in contact with SC surfaces) and often in large bundles. The axons of DRGs treated with 28 nM wild-type rLm111 were mostly segmented and in 1:1 complexes. All other conditions examined lay between the two extremes. rLm211F had a considerably higher fraction of naked axons compared to the wild-type with a distribution similar to non-polymerizing laminin and laminin lacking LG domains.

DISCUSSION

The study reveals that a partial reduction of laminin γ 1-subunit expression results in BMs with reduced levels of structural components (hence less-dense) and a SC axonal sorting defect, but without reduction of SC proliferation. In addition, increases of transcription factors (cJun, Oct6) that can contribute to hypomyelination were noted (Svaren and Meijer, 2008). The hypomorphic state was unusual in that phenotypic changes were restricted to nerve and muscle, the latter mild, despite a general reduction of laminin subunit transcription. Nerve and muscle γ 1-subunit deficiency lacked compensatory increases of other laminin subunits, in particular the Lm γ 3 subunit that is capable of joining with the same subunits as Lm γ 1. The phenotype in nerve was particularly severe, resulting in amyelination at levels comparable to the dy2J mouse. The selective defect resulting from a general transcriptional reduction suggests that a regulatory decrease in either *Lamc1* or *Lamb1* gene transcription could be a cause of selective peripheral neuropathy and myopathy in humans.

During peripheral nerve development, axonal sorting is normally accompanied by SC proliferation, the latter needed to insure availability of sufficient numbers of SCs to wrap individual axons and with both dependent upon the activity of small GTPases (Benninger et al., 2007). It is unusual that in the laminin hypomorph there was a preservation of normal SC proliferation in the face of defective radial sorting, breaking the coupling, and leaving what may be inactive SCs of indeterminate differentiation state scattered adjacent to and near naked axon bundles. Furthermore, the persistent high expression of Oct6, cJun, and Sox2 and low expression of Krox20 and MPZ as seen in the laminin-deficient nerves may reflect a deficit in the maturation of the SC

population to myelinating cells (Svaren and Meijer, 2008). The high expression level of Oct6 detected was similar to that reported in transgenic mice over-expressing Oct6, with hypomyelination present in both conditions (Ryu et al., 2007).

The normal SC proliferation of the hypomorph differs from either the *Lamc1* null or single and combined α -subunit deficient states in peripheral nerve (Yang et al., 2005; Yu et al., 2005). It was thought that the reduced BM density of the hypomorphic mouse (continuous BMs with reduced immunostaining intensity for all structural components) might represent an intermediate state in which there was sufficient BM for proliferation but not for myelination. This possibility, and a question of what laminin domain-specific activities are required for these functions, led to an examination of myelination and proliferation in laminin-deficient DRGs. The comparison revealed that the extent of BM accumulation on SC surfaces, SC proliferation, axonal ensheathment and axonal myelination was dependent on the concentration of laminin in which high laminin concentration, corresponding to high laminin expression in vivo, is more important for achieving efficient myelination than SC proliferation. The laminin-induced increase in proliferation was found to partially depend upon a contribution for the β 1-integrin-binding site (especially α 7 β 1 and α 6 β 1) in the LG domains and substantially depend upon the polymerization activity of laminins. The latter effect may be an indirect one due in part to reduced laminins and other BM component receptor-ligands and possibly to an alteration of BM rigidity, a property recently found to be involved in integrin activity and turnover (Du et al., 2011).

BMs have been proposed to act as signaling platforms in which multiple ligands are presented to cell integrin, dystroglycan and other receptors to induce changes in cell function (Li et

al., 2005). It has been further proposed that functional activation can depend upon contributions arising from ligand composition and as well as the structural properties of the scaffold itself (Engler et al., 2004; Engler et al., 2006). Laminins, however, are only among several BM components capable of providing SC integrin-binding ligands. While integrin-binding to laminin LG1-3 domains can occur with $\alpha7\beta1$ (Lm111, Lm211, Lm511), $\alpha6\beta1$ (Lm511, Lm111, and weakly with Lm411), and $\alpha3\beta1$ (Lm511), type IV collagen ($\alpha1\beta1$, $\alpha2\beta1$), perlecan ($\alpha2\beta1$) and agrin ($\alpha3\beta1$) can provide relevant integrin-binding ligands as well (Yurchenco, 2011). Non-laminin components, expressed endogenously, are recruited into the endoneurial BM upon exposure of SCs to laminins. Employing recombinant laminin that bind poorly to integrins, myelination was substantially reduced without apparent change in BM ultrastructure, or as seen in a previous study, without loss of the efficiency of accumulation of BM components on isolated SCs (McKee et al., 2007). The finding strongly suggests that direct integrin- $\beta1$ binding to laminin LG domains is a major contributor to myelination. It also adds further support to the hypothesis that integrins serve primarily as mediators of signaling and not of BM assembly in vitro (Li et al., 2002), and is consistent with the presence of BM in endoneurium in the absence of the integrin in vivo (Feltri et al., 2002).

The myelination reduction resulting from the deletion of LG4-5 is in agreement with myelination-deficient phenotype of Lm $\alpha2$ -null (*dy3K*) mouse following transgenic expression of the laminin $\alpha1$ subunit bearing a deletion of LG4-5 (Gawlik et al., 2010). Deletion of laminin LG1-3, with a predicted loss of integrin-binding, was found to reduce BM and myelination. This contribution to BM assembly was not appreciated in earlier studies (Li et al., 2002; Li et al., 2005). One possibility is that reduction of BM assembly arises from a loss of laminin binding to sulfated

glucuronate (the HNK1 epitope that binds to Lm α 1LG2) and that is expressed by SCs (Hall et al., 1997; Hall et al., 1995; Saito et al., 2005). BM coverage was restored by binding the laminin to non-neural miniagrin, a protein that attaches firmly to α -dystroglycan and sulfatides (Gesemann et al., 1998; McKee et al., 2009; Moll et al., 2001). The partial increase in myelination that accompanied this might reflect the lower affinity of miniagrin for integrin α 3 β 1 (21 nM Kd, this study) relative to Lm111 for α 6 β 1/ α 7 β 1 (9.5 and 1 nM dissociation constants respectively (Nishiuchi et al., 2006) and/or a lower abundance of α 3 β 1 compared to α 6 β 1/ α 7 β 1 in Schwann cells.

Laminin polymerization was found to contribute to both proliferation and myelination. Treatment of laminin-deficient DRGs with non-polymerizing laminins reduced BM on SC surfaces to about one-half compared to 28 nM wild-type laminin (slightly below 3.5 nM wild-type levels) and failed to support myelination. In contrast, non-polymerizing Lm Δ α 1LN-L4b did not support proliferation above no-treatment levels. The finding of a polymerization role for myelination may help explain the severity of the myelination defect of the *dy2J* mouse (Montgomery and Swenarchuk, 1978). The Lm α 2 subunit of this dystrophic mouse arises from an in-frame deletion within the Lm α 2 LN domain, destabilizing it and reducing polymerization of Lm211 (Colognato and Yurchenco, 1999; Sunada et al., 1995). The role of polymerization in myelination is primarily a structural one. Loss of the activity has been associated with reduction of laminin density in isolated SCs (McKee et al., 2007) and, here, in BM. This reduction causes a decrease in the availability of integrin-binding LG ligands and the ligands of laminin-binding proteins that may be required for myelination. Furthermore, the finding that a laminin with a selective loss of polymerization activity (i.e. rLm Δ β 1LN-LEa) demonstrates for the first time that loss

of polymerization, rather than loss of LN-dependent integrin, sulfatide, and heparin-binding, is likely to be responsible for the neuropathy.

Nidogen-1 is a structure-forming rather than receptor-binding glycoprotein with that binds to the laminin coiled-coil through its C-terminal G3 domain and to collagen-IV through its G2 and G3 domains (Fox et al., 1991; Ries et al., 2001);Salmivirta et al., 2002). Knock-in of a *Lamc1* gene coding for a laminin- γ 1 subunit lacking the L γ 1LEb3 nidogen-binding domain resulted in embryonic and early neonatal death prior to peak myelination (Willem et al., 2002). Analysis in this study of DRGs treated with laminin bearing the critical nidogen-binding L γ 1N802 mutation within domain LEb3 resulted in a slight reduction of myelination.

In conclusion, the study, through comparison of mouse and in vitro models, reveals that myelination more than SC proliferation depends upon the degree of γ 1-laminin expression/concentration within endoneurial BMs. It also demonstrated that scaffold-forming and integrin-receptor binding of laminins must act in an integrated fashion to promote axonal sorting, myelin wrapping and proliferation in which both laminin polymerization and integrin-binding through laminin LG domain substantially contribution to myelination and proliferation.

MATERIALS AND METHODS

Genetically-modified mice: Generation of conditional knockout *Lamc1* mice by flanking of exon-2 with *P-lox* (“fl”) insertions and with a retained upstream PGK*neo* selection cassette has been described (Chen and Strickland, 2003). These mice were maintained in a homozygous state (designated *Lamc1*fl^{neo}/fl^{neo}) in a C57Bl/6 background and also bred two generations into 129SvEvTac. *Lamc1*fl^{neo}/fl^{neo} males were mated with female Sox2-cre mice to create *Lamc1* +/- mice. *Lamc1* +/- Sox2-cre-negative mice were then mated with *Lamc1*fl^{neo}/fl^{neo} mice to produce *Lamc1*fl^{neo}/+ and fl^{neo}/- offspring. No difference in nerve or muscle phenotype was observed for the two backgrounds. *Lamc1*fl^{neo}/fl^{neo} mice were also bred with mice expressing FLP-recombinase (Jackson Laboratories) in order to delete the PGK*neo* cassette flanked by FRT sequences and located upstream of the LoxP inserts. Homozygous mice were mated with the +/- mice to generate *Lamc1* fl/+ and fl/- offspring that now lacked a neo cassette in the floxed gene (the neo cassette remained in the null allele). Genotyping was performed by PCR using DNA extracted from tails. Primer set 5'-CCTGGCGATCCCTGAACATGTCC and 5'-CTCTAGAGCCTCTGCTAACC was used to amplify a 300 bps product of Sox2 cre. Primer set 5'-GATTTTCAAAGAAGCAGAGTGTG and 5'-CCTACATTTTGAATGCAAGGATTGG was used to visualize a *Lamc1* floxed allele at 1.6 kb and a recombined allele at 0.6 kb. The floxed allele lacking neo was detected with primers P1-12c (5'-CTCAGAGCTGGCTTCTCCATG) and P1-6 (5'-CATTTCCCCACAAGTGGTTCTT) yielding a 400 bp wild-type product. Animal experiments were conducted according to institutional and national guidelines under protocols approved by the institutional IACUC.

Tissues, antibodies, and microscopy: (a) Tissues were embedded in OCT (Tissue-Tek, Elkhart, IN), frozen in liquid nitrogen, and stored at -80°C. Tissue-blocks were sectioned (5 µm thick) with a cryostat (Leica CM 1850) at -20°C onto charged glass slides and fixed in 3.5% paraformaldehyde for 15 min at RT or 30 min on ice. (b) Following overnight blocking (5% goat serum, 0.5% BSA, PBS) slides were treated with one or more of these antibodies: Lmγ1-subunit mAb (mouse, 1/400 dilution, Millipore), Lmβ1LN-LEa rabbit polyclonal (“anti-E4”, 1-2 µg/ml, Yurchenco et al., 1997), Lmα1LG4-5 polyclonal (5 µg/ml, Yurchenco et al., 1993). Lmα2LG1-5 rabbit polyclonal, 10 µg/ml (Cheng et al., 1997), Lmα4, 1/1000 (provided by Takako Sasaki, Oregon Health Sciences University), Lmα5, (Jeffrey Miner, Washington Univ. Sch. Medicine), Lmγ3, 1/5000 (William Brunken, Downstate Medical School), nidogen-1 rabbit polyclonal, 10 µg/ml, (Li et al., 2002), perlecan rabbit polyclonal, 2 µg/ml (Handler et al., 1997), type-IV collagen rabbit polyclonal, 0.5 µg/ml (Millipore), α-dystroglycan, mouse IgM mAb, 1/100 (Millipore/Upstate), integrin-α6 mouse mAb, 5 µg/ml (GoH3, BD Pharmingen 555734), integrin-β1 rat mAb, 10 µg/ml (MAB1997, Millipore/Upstate), neurofilament-200, 1/1000 (NFL, chicken antibody, Abcam), and myelin-basic-protein (MBP), 10 µg/ml (Millipore MAB386). DRG-derived fibroblasts were detected with anti-Thy1.2 rat IgG monoclonal antibody, 1/1000 (Thermo Scientific, MA1-90188). Bound antibodies were detected with Alexa Fluor 647 goat anti-rabbit IgG, Alexa Fluor 488 anti-mouse IgG and Alexa Fluor 594 anti-rat IgG secondary antibodies (1:100, Molecular Probes). MBP was detected anti-rat 647 and NFL detected with anti-chicken 488 (Molecular Probes a11039). For detection of nuclei, slides were stained with 2 µg/ml of Dapi (4'-6-diamidino-2-phenylindole). Cover slips were mounted with SlowFade (Invitrogen/Molecular Probes). (c) Tissues were fixed overnight in 10% neutral-buffered formalin (NBF) and embedded in paraffin. Sections were stained with hematoxylin and eosin or Mas-

son's trichrome (Tissue Analytical Service, Cancer Institute of New Jersey). **(d)** Indirect immunofluorescence and electron microscopy were performed as described (Yang et al., 2011).

Proliferation: **(a)** SC proliferation in nerve was measured by injecting pups or pregnant mice i.p. with 10 μ l/gram of 20 mM 5-ethynyl-2'-deoxyuridine (EdU) followed by harvest of sciatic nerve three hours later (Zeng et al., 2010). EdU incorporation was detected in frozen sections with the Click-iT EdU Alexa Fluor 594 imaging kit (Invitrogen, Carlsbad, CA) and counter-stained with Dapi to detect nuclei. The fraction of cells undergoing DNA-synthesis was determined by count of Edu/Dapi-staining nuclei **(b)** To measure DRG SC DNA-synthesis, cultures were incubated with 1 μ M EdU for 3 hrs, washed, fixed in 3.7% paraformaldehyde, permeabilized with 0.1% Triton-X100, reacted with Click-iT Alexa-594 dye-conjugate, and counterstained with Dapi. EdU/Dapi ratios were estimated by segmentation analysis.

Quantitative real-time PCR analysis: RNA was isolated and stabilized from tissues with reagents provided by an RNeasy Plus Mini kit (Qiagen). Real-time reverse-transcriptase polymerase chain reaction (qRT-PCR) was carried out to quantify laminin subunits, integrin β 1, perlecan, c-Jun, Oct6/Scip, Krox-20, myelin protein zero (MPZ), p75-NTR, neuregulin-1, ErbB2 and FGF2 by using an ABI 7900 HT Sequence Detection System as described (Yang et al., 2011).

Recombinant and other glycoproteins: **(a)** Type IV collagen (Col-IV) was purified from the Engelbreth-Holm-Swarm (EHS) tumor as described (Yurchenco and Furthmayr, 1984). **(b)** Recombinant glycoproteins: rLm111, rLm111 bearing a γ 1-subunit C-terminal Flag tag (rLm111F), rLm111 with a deletion of LG domains 1-3 and containing Flag (rLm Δ α 1LG1-3), rLm111 with a

deletion of LG domains 4-5 without Flag (rLm $\Delta\alpha$ 1LG4-5), rLm111 with deletion of α 1-subunit short arm domains LN through L4b (rLm $\Delta\alpha$ 1LN-L4b) without Flag, rLm111 with deletion of β 1-subunit short arm domains LN-LEa (rLm $\Delta\beta$ 1LN-LEa) without Flag, rLm111 with a γ 1N802S mutation without Flag, nidogen-1 (rNd1) and non-neural miniagrin (mA) were prepared in HEK293 cells and purified as described (McKee et al., 2009; McKee et al., 2007). To generate deletion mutants of the Lm α 1 chain for domains LG1-3 and LG4-5, an XhoI digest of the mouse α 1 plasmid removed a 4.8kb fragment leaving a 9.4Kb fragment. The LG1-3 deletion construct required overlapping PCR utilizing primer pairs “P1F” and “P2R” (5’GAAAGGTGCTGTGCAGGCTATCACG and 5’GAGTTCCCCGTGTTCTCTGTGCAGTGTTCGGGCCCGGCTGATCAGCAG) and “P2F” and “P1R” (5’CTGCTGATCAGCCGGGCCCGGAAACACTGCACAGAGAACACGGGGA ACTC and 5’GCTGATCAGCGGGTTTAAACGGGC). The generated 1.8Kb and 1.2Kb products were sewn together with primers P1F and P1R, digested with XhoI and ligated to the 9.4 Kb fragment. The LG4-5 deletion was generated with a single PCR product using P1F and P3R (5’GATGCGGCTCGAGTTATCAACTCTGCATGGGCTCTTCTGCCAG) and includes 2 stop codons and an XhoI site downstream of LG3. The 3.6Kb PCR product was digested with XhoI and ligated into the 9.4Kb fragment. To generate cells expressing Lm211 without a Flag epitope-tag, stable Lm γ 1/Lm β 1-expressing HEK293 cells were transfected with pCis-human Lm α 2 DNA and pcDNA3.1-puro as described (McKee et al., 2007; Smirnov et al., 2002). (c) Protein was purified with HA-affinity gel (Sigma E677) as per the manufacture conditions. Laminin-211 bearing a γ 1-subunit C-terminal Flag epitope-tag (rLm-211F) was prepared as described (Smirnov et al., 2002). Laminin concentrations were determined from intensity of Coomassie-blue stained

aliquots whose bands were separated by SDS-PAGE (reducing conditions) against EHS-Lm111 standards and using the following peptide molecular masses to calculate molar concentrations (McKee et al., 2007; Yurchenco and Cheng, 1993).

Dorsal root ganglia and Schwann cell cultures (a) Dorsal root ganglia (DRGs) were isolated by dissection from *Lamc1fl^{neo}/fl^{neo}* embryos at E13.5 based on the method of Paivalainen et al., 2008. One to two DRGs were placed into each collagen-treated tissue culture well (24-well dishes, treated with 2 mg/ml rat tail collagen in 0.1 M acetic acid and neutralized with ammonium hydroxide vapors) along with 20 μ l of growth medium/well, and allowed to adhere followed by addition of 0.3 ml medium. The DRGs were treated 3 days later with 2×10^7 PFU of cre-recombinase-GFP adenovirus (DNA kindly provided by Tse-Hua Tan, Baylor College (Grewal et al., 2001) with virus generated in HEK293 cells and purified by CsCl density-gradient centrifugation). GFP fluorescence was used to determine optimal viral titer and to confirm expression of recombinase. Recombinant nidogen-1 (28 nM), with or without recombinant laminins were added at the same time as virus. After 3 additional days, the initial medium was replaced with myelination media containing ascorbic acid, and including different recombinant proteins. Media was changed every 3 days for a total of 6 days. DRGs were then fixed for 15 minutes with 3.5% paraformaldehyde (RT), treated for 6 min with ice-cold methanol, followed by blocking buffer containing 0.1% Triton X-100 overnight at 4°C. DRGs were then stained with antibodies.

(b) For isolation of SCs for adhesion assays, multiple DRGs were placed in a single collagen-coated dish and maintained in growth medium for 7-10 days. SCs were passaged in SC medium at a density of 1.5×10^6 /100 mm dish and used at passage 5-6 for adhesion assays. Fibroblast contamination levels were determined by Thy1.2 antibody and Dapi staining. The antibody-

stained cells were broad and flat unlike the fusiform Schwann cells. The cells used to evaluate cell adhesion were found to contain $0.7 \pm 0.3\%$ fibroblasts (average and S.D. of five microscope fields, total of 1762 cells).

Image Analysis: (a) Overlapping images (4x objective) of immuno-stained DRGs were recorded in IPLab and joined to create a composite image. The degree of DRG myelination was estimated from these images by several methods. (i) The first was by determining the ratio of myelinated axons stained red with MBP to NFL-stained axons and gfp-fluorescing SCs (green) by segmentation analysis of photographed images in IPLab. A common baseline level to subtract non-specific fluorescence was established for each fluor within the group of DRGs to be analyzed. The segmentation parameters for myelin and axons were set to identify a maximum number of myelinated or axonal forms respectively while minimizing background. Segmented images were then used to determine values for the sum of pixel intensities. An average of three or more DRGs per condition were used to calculate an average and standard deviation. (ii) The second method was by direct measurement of the lengths of myelinated forms contained within a DRG. This was accomplished by tracing the linear myelinated (MBP-stained) structures and recording the accumulation of linear pixels with the IPLab application for this purpose. The summed lengths were divided by the area of the DRG delineated by the NFL/gfp stained structures and expressed as an average and standard deviation for the DRGs for each condition evaluated. (iii) The distribution of myelinated segment lengths was determined by sampling MBP-stained segments whose ends could be clearly distinguished. (b) Proliferation was estimated in a similar manner in DRGs by determining the ratio of EdU stained nuclei (red) to total Dapi-stained nuclei (blue). (c) Electron micrograph measurements were performed by tracing structures of interest in either IPLab (v.3.7,

Scanalytics) in Windows or iVision (v.4.0.15, BioVision Technologies) with calculations performed in Excel. The ratio of axonal and axonal and myelin areas and distribution of axonal areas, were calculated from multiple (2300 – 3000x magnification) cross-section images. The ratio of BM/plasma membrane was determined after tracing contour lengths of each along multiple SC surfaces containing BMs.

Cell adhesion and integrin-binding assays: (a) Costar 96-well polystyrene dishes (#3631) were coated with BM proteins in 0.15 M sodium bicarbonate (pH 9.6) overnight at 4°C. Plates were washed and blocked for 1 hr at RT with 0.3% heat-inactivated BSA in PBS. SCs (30,000 cells/100ul/well) were allowed to adhere for 80 min. Unbound cells were removed with three PBS washes and WST-1 (Clontech) was added at 1/10 into SC media. Adherent cells were measured by absorption (492nm) in a Tecan Spectra Fluor. (b) Integrin binding to recombinant laminins and miniagrin immobilized in 96-well dishes was determined with recombinant extracellular domains of integrins basically as described (Nishiuchi et al., 2006). In brief, integrins $\alpha 6\beta 1$, $\alpha 7\beta 1$, $\alpha 3\beta 1$ and $\alpha v\beta 1$ were fused to ACID/BASE α -helical peptides with FLAG/6His epitope tags and containing cysteines for disulfide-bonding of subunit fragments. Plastic wells were coated with laminins (20 μ g/ml, 2-3 hrs) in TBS, blocked with 3% BSA containing 0.1% Tween-20 (1 hr), and incubated with the soluble integrins at different concentrations for 2 hr at RT in Tris-buffered saline (TBS: 50 mM Tris-HCl, 90 mM NaCl, pH 7.4) containing 1mM manganese sulfate, 0.1% Tween-20. After washing, the wells were incubated with biotinylated rabbit anti-Velcro antibody (ACID/BASE coiled-coil, 1:1000 dilution), followed by HRP-conjugated streptavidin (1 μ g/ml). Binding was detected by incubating with o-phenylenediamine with absorbance measured at 492 nm.

Acknowledgements: This study was supported by grants to PDY (NIH grants R37-DK36425 and R01-NS38469), ZLC (Muscular Dystrophy Association grant #MDA4066) and SS (NIH grant NS038472). We thank Bruce Patton (Oregon Health Sciences University) for help in examining nerve and muscle pathology and useful discussions and David Harrison and Sergei Smirnov (Robert W Johnson Medical School) for construct design and integrin-binding assays.

FIGURE LEGENDS

Figure 1. *Sciatic nerve.* Panels A-F. Methylene blue stained semi-thin longitudinal (A,D) and cross-sections (B,C,E,F) of sciatic nerve (sn, A,B,D,E) and sciatic nerve root (snr, C,F) of *Lmγ1 fl^{neo/+}* (A-C) and *Lmγ1 fl^{neo/-}* (B,D) adult (12 old week) mice. The *fl^{neo/-}* nerve and root contain a patchy distribution of unmyelinated axons, most pronounced in the roots. In addition, the myelin had many infoldings (inset, arrows). Panels G-J. Electron micrograph of *Lmγ1 fl^{neo/-}* (H) nerve reveals bundles of naked axons and nearby and adjacent non-myelinating SCs (arrows) not seen in *fl^{neo/+}* littermate nerve (G). Endoneurial BMs were continuous with similar thickness in *fl^{neo/+}* (I) and *Lmγ1 fl^{neo/-}* (J) SCs.

Figure 2. *Laminin expression.* **A.** Comparison of laminin mRNA by quantitative real time RT-PCR revealed *Lmγ1 fl^{neo/-}* mRNA was decreased about three-fold compared to wild-type controls in nerve, muscle and other tissues. Lesser reductions were detected for +/- tissues (plots are average and standard deviation of experiments performed in triplicate using RNA from 5 mice from each genotype). **B.** Immunofluorescence images of *fl^{neo/-}* adult sciatic nerve reveal decreases in laminin subunits, perlecan (perl), and collagen-IV (ColIV), but not integrin subunits (Itgβ1, Itgα6), or α-dystroglycan compared to *fl^{neo/+}* littermates.

Figure 3. *Schwann cell proliferation and myelination factors.* Panels A-D: Hindlimb nerve from *fl^{neo/+}* and *fl^{neo/-}* embryos (E18.5, A,B) and post-natal day 1 pups littermates (C,D) were labeled with EdU and stained with Dapi to compare DNA synthesis (shown with NFL counter-stain, green). Panels E-F: Sciatic nerve from 10 wk old *fl^{neo/+}* (E) and *fl^{neo/-}* (F) littermates were

stained with Dapi and NFL antibody. Collections of NFL-stained axons characteristic of the mutant state are seen in F. Panels G-I: The fraction of EdU-positive (red) Dapi-stained (blue) nuclei in nerves was determined (average and standard deviation of three pairs) at E18.5 (G) and P1 (H). No significant difference was detected. I: Nuclear count per nerve section was similar in $fl^{neo/+}$ and $fl^{neo/-}$ -adults. Panels J,K. Steady-state mRNA levels of myelination factors. Proximal sciatic nerve segments were isolated from adult (A) and P5 (B) mice followed by RNA extraction and quantitative real-time reverse-transcriptase PCR for mRNA ($fl^{neo/-}$ to $fl^{neo/+}$ ratio) transcribing the indicated proteins (number of samples indicated with small digits in graphs). Reductions in mutant nerves were identified for laminin- γ 1 (LmC1), Krox-20, MPZ, p75, and neuregulin-1 (Nrg1). Elevations were identified for c-Jun, Oct-6 and Sox2. The patterns were similar at both stages.

Figure 4. *Laminin domains and activities.* **A.** Map of cell-surface-glycolipid attachment sites, integrin-binding, α -dystroglycan (DG) binding, polymerization (polym.), nidogen (Nd) binding and heparan sulfate (HS) binding activities of Lm111. **B.** Recombinant laminins bearing modifications that reduce and ablate nidogen-binding, laminin polymerization, integrin-binding through LG domains, and cell-surface-adhesion are shown. α LNNd (F1) is a linker protein that binds to Lms at the nidogen-binding locus, adding the α 1LN polymerization domain. **C.** Schematic diagram of Lmy1 C-terminal sequence (violet) with critical glutamic acid residue (red) thought to interact with LG domains, followed by the Flag-tag sequence (yellow) that interferes with integrin binding.

Figure 5. *Laminin-dependent Schwann cell proliferation and myelination in DRG cultures.* *Lamc1-fl^{neo}/fl^{neo}* DRGs, isolated from E13.5 pregnant females and rendered laminin-deficient with adeno-cre recombinase virus, were treated with the different concentrations of rLm111 (0, 3.5, 7, 14, and 28 nM, panels A-J) followed by evaluation for proliferation (ratio of MBP/NFL+gfp, panels, panels A-E) at day 0 and myelination (ratio of EdU/Dapi; panels A-D) at day 6. The corresponding plots for proliferation (K) and myelination induced (L) are shown (average and S.D. of 3-5 DRGs). While myelination and proliferation both depended on laminin concentration, proliferation increased at low levels and reached a plateau by 28 nM while myelination continued to increase over the full concentration range.

Figure 6. *Schwann cell adhesion to basement membrane components and integrin-binding.* Panels A-B. Schwann cells isolated from DRGs were expanded in culture and evaluated for adhesion to plastic well coated with laminins and other BM substrates. **A.** Adhesion to rLm-111 (closed circles), collagen-IV (Col-IV, open inverted triangles), rNd1 (open inverted diamonds), rLm $\Delta\alpha$ 1LG1-3 (open hexagons), and miniagrin (mA, open squares) shown (average and S.D., n=4). **B.** Adhesion of cells to rLm-111 (closed circles) and rLm-211 (closed triangles) and corresponding flag-tagged rLm-111F (open circles) and rLm-211F (open triangles). Higher coat concentrations were required to achieve similar adhesion for Flag-tagged laminins. Panels C-F. Binding of soluble-integrin-ectodomain-dimers to wild-type and Flag-tagged rLm-211 (**C**), and to correspondingly-modified rLm-111 (**D, E**). Five to ten fold reductions of binding affinity were detected for Flag-tagged laminins for integrins α 7 β 1 and α 6 β 1. (**F**). Miniagrin (mA), containing

LG cell-adhesion domains, bound to integrin $\alpha 3\beta 1$ closed circles; $\alpha 6\beta 1$ open diamonds; $\alpha v\beta 1$, open circles; $\alpha 7\beta 1X2$, open inverted triangles; $\alpha 7\beta 1X1$, open squares; $\alpha 5\beta 1$, open triangles).

Figure 7. *DRG myelination in response to functional modifications of laminins.* **A.** Composite images of Lm-deficient DRGs cultured with 28 nM recombinant laminins and nidogen, immunostained for MBP (red) and NFL (green). **B.** Plot of myelination (ratio of MBP/NFL+gfp, average and S.D. for indicated number of DRGs) showing reductions in DRGs treated with C-terminal Flag-tagged laminins and ablation of polymerization through deletion of LN-containing segments of either the $\alpha 1$ or $\beta 1$ subunit eliminated myelination. Myelination was substantially increased by treating rLm $\Delta\alpha$ LN-L4b with α LNNd. A partial (but not statistically significant, P=0.1) loss of myelination was seen with laminin unable to bind nidogen. Deletion of either the proximal or distal LG-domains ablated myelination. **C.** Laminin-deficient DRGs treated with 28 nM rLm111 were sectioned and immunostained for laminin-subunits, perlecan and collagen-IV. **D.** Comparison (average and S.D., 5 DRGs/condition) of Schwann cell proliferation in response to rLm211F (closed squares, upper plot) compared to wild-type rLm211 (closed circles), and comparison of cell proliferation in response to rLm $\Delta\alpha$ LN-L4b (closed squares, lower plot) compared to wild-type rLm111 (closed circles). Presence of the Flag-tagged reduced proliferation while loss of polymerization completely prevented proliferation above baseline (no added laminin) levels for all concentrations.

Figure 8. *DRG ultrastructure.* Laminin-deficient DRGs treated with the indicated laminins. Panels A-E. DRG maintained with no added laminin (**A**), 3.5 nM rLm111 (**B**), 7 nM rLm-111 (**C**), and 28 nM rLm111 (**D**), and 28 nM rLm211 (**E**). Nearly all axons were naked (nAx), often in

small bundles) in the absence of added laminin. Axons were enveloped (eAx) or myelinated (mAx) following treatment with recombinant laminins, with myelin wrapping more prominent at higher concentrations. Insets magnified to show BM (arrows), gaps (asterisks) and plasma membrane (white arrowheads). **F.** Plot of BM coverage on cell surfaces (BM/plasma membrane ratio, average and S.D. for 8-12 images) after treatment of DRGs with rLm111 reveals increasing BM as laminin concentration increased. **G.** Plot of BM/PM ratio for DRGs treated with the laminins bearing domain-modifications.

REFERENCES

- Ard, M. D., Bunge, R. P. and Bunge, M. B.** (1987). Comparison of the Schwann cell surface and Schwann cell extracellular matrix as promoters of neurite growth. *J. Neurocytol.* **16**, 539-555.
- Benninger, Y., Thurnherr, T., Pereira, J. A., Krause, S., Wu, X., Chrostek-Grashoff, A., Herzog, D., Nave, K. A., Franklin, R. J., Meijer, D. et al.** (2007). Essential and distinct roles for cdc42 and rac1 in the regulation of Schwann cell biology during peripheral nervous system development. *J Cell Biol* **177**, 1051-61.
- Berti, C., Bartesaghi, L., Ghidinelli, M., Zambroni, D., Figlia, G., Chen, Z. L., Quattrini, A., Wrabetz, L. and Feltri, M. L.** (2011). Non-redundant function of dystroglycan and beta1 integrins in radial sorting of axons. *Development* **138**, 4025-37.
- Bunge, R. P., Bunge, M. B. and Eldridge, C. F.** (1986). Linkage between axonal ensheathment and basal lamina production by Schwann cells. *Annu.Rev.Neurosci.* **9**, 305-328.
- Chen, Z. L. and Strickland, S.** (2003). Laminin gamma1 is critical for Schwann cell differentiation, axon myelination, and regeneration in the peripheral nerve. *J Cell Biol* **163**, 889-899.
- Cheng, Y. S., Champlaud, M. F., Burgeson, R. E., Marinkovich, M. P. and Yurchenco, P. D.** (1997). Self-assembly of laminin isoforms. *J Biol Chem* **272**, 31525-32.
- Clark, M. B. and Bunge, M. B.** (1989). Cultured Schwann cells assemble normal-appearing basal lamina only when they ensheath axons. *Dev Biol* **133**, 393-404.
- Colognato-Pyke, H., O'Rear, J. J., Yamada, Y., Carbonetto, S., Cheng, Y. S. and Yurchenco, P. D.** (1995). Mapping of network-forming, heparin-binding, and alpha 1 beta 1 integrin-recognition sites within the alpha-chain short arm of laminin- 1. *J. Biol. Chem.* **270**, 9398-406.
- Colognato, H. and Yurchenco, P. D.** (1999). The laminin alpha2 expressed by dystrophic dy(2J) mice is defective in its ability to form polymers. *Curr Biol* **9**, 1327-1330.
- Du, J., Chen, X., Liang, X., Zhang, G., Xu, J., He, L., Zhan, Q., Feng, X. Q., Chien, S. and Yang, C.** (2011). Integrin activation and internalization on soft ECM as a mechanism of induction of stem cell differentiation by ECM elasticity. *Proc Natl Acad Sci U S A* **108**, 9466-71.
- Eldridge, C. F., Bunge, M. B. and Bunge, R. P.** (1989). Differentiation of axon-related Schwann cells in vitro: II. Control of myelin formation by basal lamina. *J Neurosci* **9**, 625-38.
- Eldridge, C. F., Bunge, M. B., Bunge, R. P. and Wood, P. M.** (1987). Differentiation of axon-related Schwann cells in vitro. I. Ascorbic acid regulates basal lamina assembly and myelin formation. *J Cell Biol* **105**, 1023-34.
- Engler, A., Bacakova, L., Newman, C., Hategan, A., Griffin, M. and Discher, D.** (2004). Substrate compliance versus ligand density in cell on gel responses. *Biophys J* **86**, 617-28.
- Engler, A. J., Sen, S., Sweeney, H. L. and Discher, D. E.** (2006). Matrix elasticity directs stem cell lineage specification. *Cell* **126**, 677-89.
- Feltri, M. L., Graus Porta, D., Previtali, S. C., Nodari, A., Migliavacca, B., Casseti, A., Littlewood-Evans, A., Reichardt, L. F., Messing, A., Quattrini, A. et al.** (2002). Conditional disruption of beta 1 integrin in Schwann cells impedes interactions with axons. *J Cell Biol* **156**, 199-209.

- Fox, J. W., Mayer, U., Nischt, R., Aumailley, M., Reinhardt, D., Wiedemann, H., Mann, K., Timpl, R., Krieg, T., Engel, J. et al.** (1991). Recombinant nidogen consists of three globular domains and mediates binding of laminin to collagen type IV. *EMBO. J.* **10**, 3137-3146.
- Gawlik, K. I., Akerlund, M., Carmignac, V., Elamaa, H. and Durbeej, M.** (2010). Distinct roles for laminin globular domains in laminin alpha1 chain mediated rescue of murine laminin alpha2 chain deficiency. *PLoS ONE* **5**, e11549.
- Gawlik, K. I., Li, J. Y., Petersen, A. and Durbeej, M.** (2006). Laminin alpha1 chain improves laminin alpha2 chain deficient peripheral neuropathy. *Hum Mol Genet* **15**, 2690-700.
- Gesemann, M., Brancaccio, A., Schumacher, B. and Ruegg, M. A.** (1998). Agrin is a high-affinity binding protein of dystroglycan in non-muscle tissue. *J Biol Chem* **273**, 600-5.
- Grewal, P. K., Holzfeind, P. J., Bittner, R. E. and Hewitt, J. E.** (2001). Mutant glycosyltransferase and altered glycosylation of alpha-dystroglycan in the myodystrophy mouse. *Nat Genet* **28**, 151-4.
- Hall, H., Deutzmann, R., Timpl, R., Vaughan, L., Schmitz, B. and Schachner, M.** (1997). HNK-1 carbohydrate-mediated cell adhesion to laminin-1 is different from heparin-mediated and sulfatide-mediated cell adhesion. *Eur J Biochem* **246**, 233-42.
- Hall, H., Vorherr, T. and Schachner, M.** (1995). Characterization of a 21 amino acid peptide sequence of the laminin G2 domain that is involved in HNK-1 carbohydrate binding and cell adhesion. *Glycobiology* **5**, 435-41.
- Handler, M., Yurchenco, P. D. and Iozzo, R. V.** (1997). Developmental expression of perlecan during murine embryogenesis. *Dev Dyn* **210**, 130-45.
- Harrison, D., Hussain, S. A., Combs, A. C., Ervasti, J. M., Yurchenco, P. D. and Hohenester, E.** (2007). Crystal structure and cell surface anchorage sites of laminin alpha 1LG4-5. *J Biol Chem* **282**, 11573-11581.
- Ido, H., Nakamura, A., Kobayashi, R., Ito, S., Li, S., Futaki, S. and Sekiguchi, K.** (2007). The requirement of the glutamic acid residue at the third position from the carboxyl termini of the laminin gamma chains in integrin binding by laminins. *J Biol Chem* **282**, 11144-54.
- Li, S., Harrison, D., Carbonetto, S., Fassler, R., Smyth, N., Edgar, D. and Yurchenco, P. D.** (2002). Matrix assembly, regulation, and survival functions of laminin and its receptors in embryonic stem cell differentiation. *J Cell Biol* **157**, 1279-90.
- Li, S., Liquari, P., McKee, K. K., Harrison, D., Patel, R., Lee, S. and Yurchenco, P. D.** (2005). Laminin-sulfatide binding initiates basement membrane assembly and enables receptor signaling in Schwann cells and fibroblasts. *J Cell Biol* **169**, 179-89.
- Ma, Z., Wang, J., Song, F. and Loeb, J. A.** (2011). Critical period of axoglial signaling between neuregulin-1 and brain-derived neurotrophic factor required for early Schwann cell survival and differentiation. *J Neurosci* **31**, 9630-40.
- McKee, K. K., Capizzi, S. and Yurchenco, P. D.** (2009). Scaffold-forming and adhesive contributions of synthetic laminin-binding proteins to basement membrane assembly. *J Biol Chem* **284**, 8984-8994.
- McKee, K. K., Harrison, D., Capizzi, S. and Yurchenco, P. D.** (2007). Role of laminin terminal globular domains in basement membrane assembly. *J Biol Chem* **282**, 21437-47.
- Meyers, E. N., Lewandoski, M. and Martin, G. R.** (1998). An Fgf8 mutant allelic series generated by Cre- and Flp-mediated recombination. *Nat Genet* **18**, 136-41.
- Moll, J., Barzaghi, P., Lin, S., Bezakova, G., Lochmuller, H., Engvall, E., Muller, U. and Ruegg, M. A.** (2001). An agrin minigene rescues dystrophic symptoms in a mouse model for congenital muscular dystrophy. *Nature* **413**, 302-7.

- Montgomery, A. and Swenarchuk, L.** (1978). Further observations on myelinated axon numbers in normal and dystrophic mice. *J Neurol Sci* **38**, 77-82.
- Nishiuchi, R., Takagi, J., Hayashi, M., Ido, H., Yagi, Y., Sanzen, N., Tsuji, T., Yamada, M. and Sekiguchi, K.** (2006). Ligand-binding specificities of laminin-binding integrins: A comprehensive survey of laminin-integrin interactions using recombinant alpha3beta1, alpha6beta1, alpha7beta1 and alpha6beta4 integrins. *Matrix Biol* **25**, 189-197.
- Nodari, A., Previtali, S. C., Dati, G., Occhi, S., Court, F. A., Colombelli, C., Zambroni, D., Dina, G., Del Carro, U., Campbell, K. P. et al.** (2008). Alpha6beta4 integrin and dystroglycan cooperate to stabilize the myelin sheath. *J Neurosci* **28**, 6714-9.
- Nodari, A., Zambroni, D., Quattrini, A., Court, F. A., D'Urso, A., Recchia, A., Tybulewicz, V. L., Wrabetz, L. and Feltri, M. L.** (2007). Beta1 integrin activates Rac1 in Schwann cells to generate radial lamellae during axonal sorting and myelination. *J Cell Biol* **177**, 1063-75.
- Paivalainen, S., Nissinen, M., Honkanen, H., Lahti, O., Kangas, S. M., Peltonen, J., Peltonen, S. and Heape, A. M.** (2008). Myelination in mouse dorsal root ganglion/Schwann cell cocultures. *Mol Cell Neurosci* **37**, 568-78.
- Pereira, J. A., Benninger, Y., Baumann, R., Goncalves, A. F., Ozcelik, M., Thurnherr, T., Tricaud, N., Meijer, D., Fassler, R., Suter, U. et al.** (2009). Integrin-linked kinase is required for radial sorting of axons and Schwann cell remyelination in the peripheral nervous system. *J Cell Biol* **185**, 147-61.
- Ries, A., Gohring, W., Fox, J. W., Timpl, R. and Sasaki, T.** (2001). Recombinant domains of mouse nidogen-1 and their binding to basement membrane proteins and monoclonal antibodies. *Eur J Biochem* **268**, 5119-28.
- Ryu, E. J., Wang, J. Y., Le, N., Baloh, R. H., Gustin, J. A., Schmidt, R. E. and Milbrandt, J.** (2007). Misexpression of Pou3f1 results in peripheral nerve hypomyelination and axonal loss. *J Neurosci* **27**, 11552-9.
- Saito, F., Moore, S. A., Barresi, R., Henry, M. D., Messing, A., Ross-Barta, S. E., Cohn, R. D., Williamson, R. A., Sluka, K. A., Sherman, D. L. et al.** (2003). Unique role of dystroglycan in peripheral nerve myelination, nodal structure, and sodium channel stabilization. *Neuron* **38**, 747-58.
- Saito, H., Nakao, Y., Takayama, S., Toyama, Y. and Asou, H.** (2005). Specific expression of an HNK-1 carbohydrate epitope and NCAM on femoral nerve Schwann cells in mice. *Neurosci Res* **53**, 314-22.
- Salmivirta, K., Talts, J., Olsson, M., Sasaki, T., Timpl, R. and Ekblom, P.** (2002). Binding of mouse nidogen-2 to basement membrane components and cells and its expression in embryonic and adult tissues suggest complementary functions of the two nidogens. *Exp Cell Res* **279**, 188.
- Shannon, M. B., Patton, B. L., Harvey, S. J. and Miner, J. H.** (2006). A hypomorphic mutation in the mouse laminin alpha5 gene causes polycystic kidney disease. *J Am Soc Nephrol* **17**, 1913-22.
- Smirnov, S. P., McDearmon, E. L., Li, S., Ervasti, J. M., Tryggvason, K. and Yurchenco, P. D.** (2002). Contributions of the LG Modules and Furin Processing to Laminin-2 Functions. *J Biol Chem* **277**, 18928-18937.
- Smyth, N., Vatansver, H. S., Murray, P., Meyer, M., Frie, C., Paulsson, M. and Edgar, D.** (1999). Absence of Basement Membranes after Targeting the LAMC1 Gene Results in Embryonic Lethality Due to Failure of Endoderm Differentiation. *J Cell Biol* **144**, 151-160.

- Sunada, Y., Bernier, S. M., Utani, A., Yamada, Y. and Campbell, K. P.** (1995). Identification of a novel mutant transcript of laminin alpha 2 chain gene responsible for muscular dystrophy and dysmyelination in dy2J mice. *Hum Mol Genet* **4**, 1055-61.
- Sung, U., O'Rear, J. J. and Yurchenco, P. D.** (1993). Cell and heparin binding in the distal long arm of laminin: identification of active and cryptic sites with recombinant and hybrid glycoprotein. *J. Cell. Biol.* **123**, 1255-1268.
- Svaren, J. and Meijer, D.** (2008). The molecular machinery of myelin gene transcription in Schwann cells. *Glia* **56**, 1541-51.
- Webster, H. D.** (1971). The geometry of peripheral myelin sheaths during their formation and growth in rat sciatic nerves. *J Cell Biol* **48**, 348-67.
- Webster, H. d.** (1993). Development of peripheral nerve fibers. In *Peripheral Neuropathy*, vol. 1 (eds P. J. Dyke and P. K. Thomas), pp. 243-266. Philadelphia: W.B. Saunders Company.
- Webster, H. D., Martin, R. and O'Connell, M. F.** (1973). The relationships between interphase Schwann cells and axons before myelination: a quantitative electron microscopic study. *Dev Biol* **32**, 401-16.
- Willem, M., Miosge, N., Halfter, W., Smyth, N., Jannetti, I., Burghart, E., Timpl, R. and Mayer, U.** (2002). Specific ablation of the nidogen-binding site in the laminin gamma1 chain interferes with kidney and lung development. *Development* **129**, 2711-2722.
- Yang, D., Bierman, J., Tarumi, Y. S., Zhong, Y. P., Rangwala, R., Proctor, T. M., Miyagoe-Suzuki, Y., Takeda, S., Miner, J. H., Sherman, L. S. et al.** (2005). Coordinate control of axon defasciculation and myelination by laminin-2 and -8. *J Cell Biol* **168**, 655-666.
- Yang, D. H., McKee, K. K., Chen, Z. L., Mernaugh, G., Strickland, S., Zent, R. and Yurchenco, P. D.** (2011). Renal collecting system growth and function depend upon embryonic {gamma}1 laminin expression. *Development* **138**, 4535-44.
- Yu, W. M., Chen, Z. L., North, A. J. and Strickland, S.** (2009). Laminin is required for Schwann cell morphogenesis. *J Cell Sci* **122**, 929-36.
- Yu, W. M., Feltri, M. L., Wrabetz, L., Strickland, S. and Chen, Z. L.** (2005). Schwann cell-specific ablation of laminin gamma1 causes apoptosis and prevents proliferation. *J Neurosci* **25**, 4463-72.
- Yurchenco, P. D.** (2011). Basement membranes: cell scaffoldings and signaling platforms. *Cold Spring Harb Perspect Biol* **3**, a004911.
- Yurchenco, P. D. and Cheng, Y. S.** (1993). Self-assembly and calcium-binding sites in laminin. A three-arm interaction model. *J. Biol. Chem.* **268**, 17286-17299.
- Yurchenco, P. D. and Furthmayr, H.** (1984). Self-assembly of basement membrane collagen. *Biochemistry* **23**, 1839-50.
- Yurchenco, P. D., Quan, Y., Colognato, H., Mathus, T., Harrison, D., Yamada, Y. and O'Rear, J. J.** (1997). The alpha chain of laminin-1 is independently secreted and drives secretion of its beta- and gamma-chain partners. *Proc Natl Acad Sci U S A* **94**, 10189-94.
- Yurchenco, P. D., Sung, U., Ward, M. D., Yamada, Y. and O'Rear, J. J.** (1993). Recombinant laminin G domain mediates myoblast adhesion and heparin binding. *J. Biol. Chem.* **268**, 8356-8365.
- Zeng, C., Pan, F., Jones, L. A., Lim, M. M., Griffin, E. A., Sheline, Y. I., Mintun, M. A., Holtzman, D. M. and Mach, R. H.** (2010). Evaluation of 5-ethynyl-2'-deoxyuridine staining as a sensitive and reliable method for studying cell proliferation in the adult nervous system. *Brain Res* **1319**, 21-32.

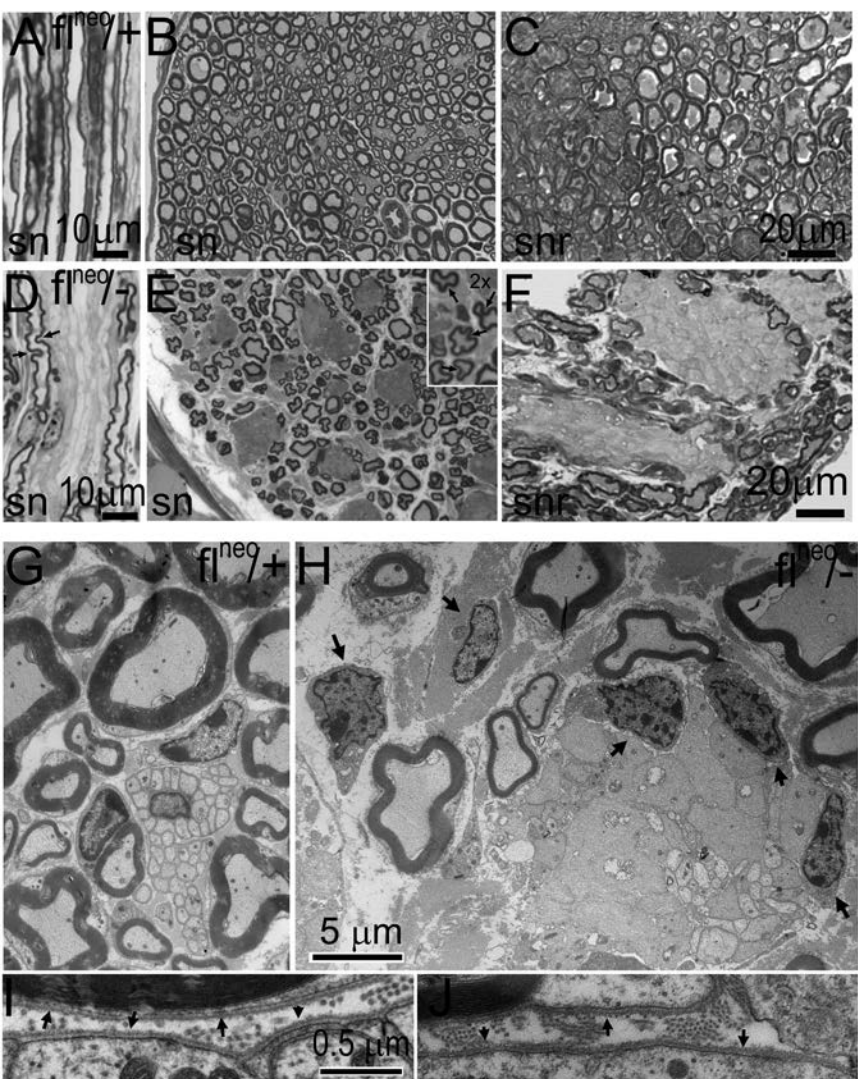


Fig. 1

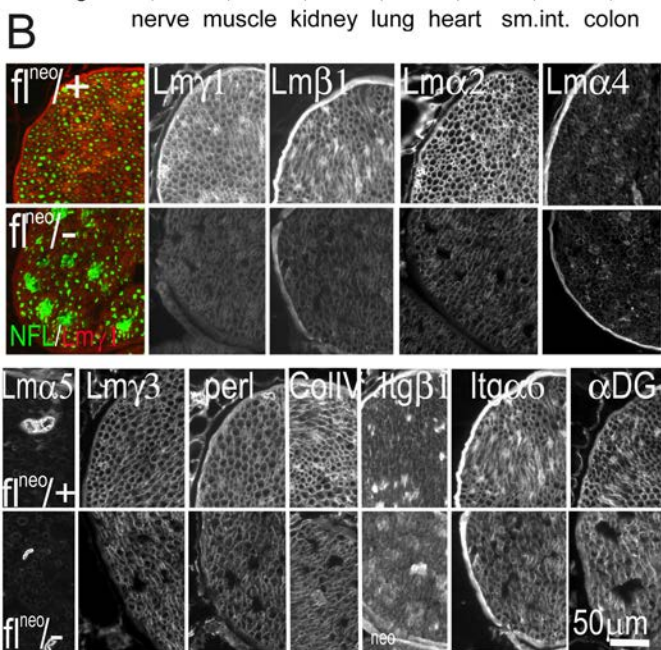
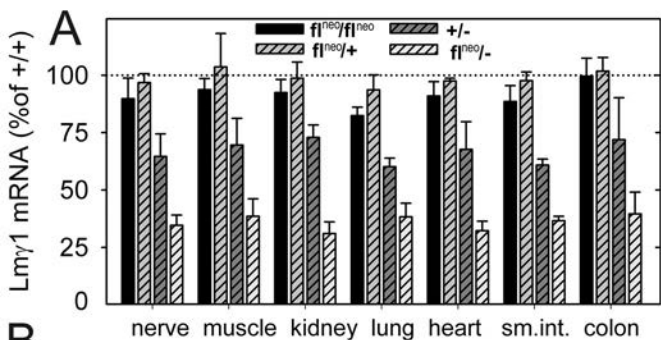


Fig. 2

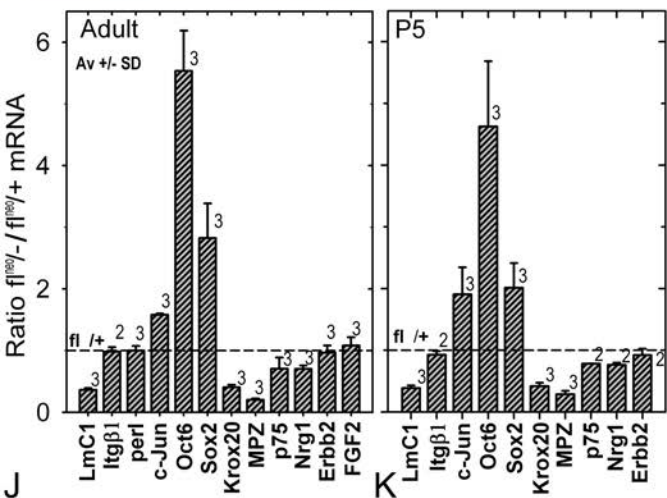
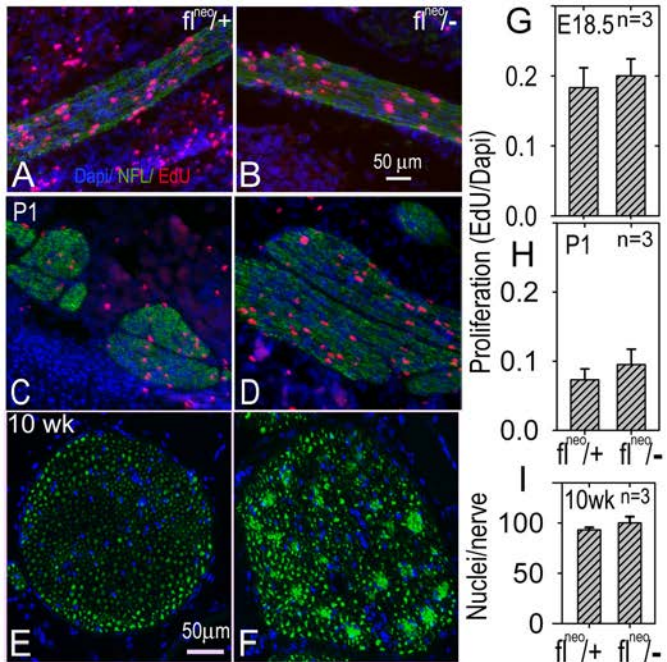


Fig. 3

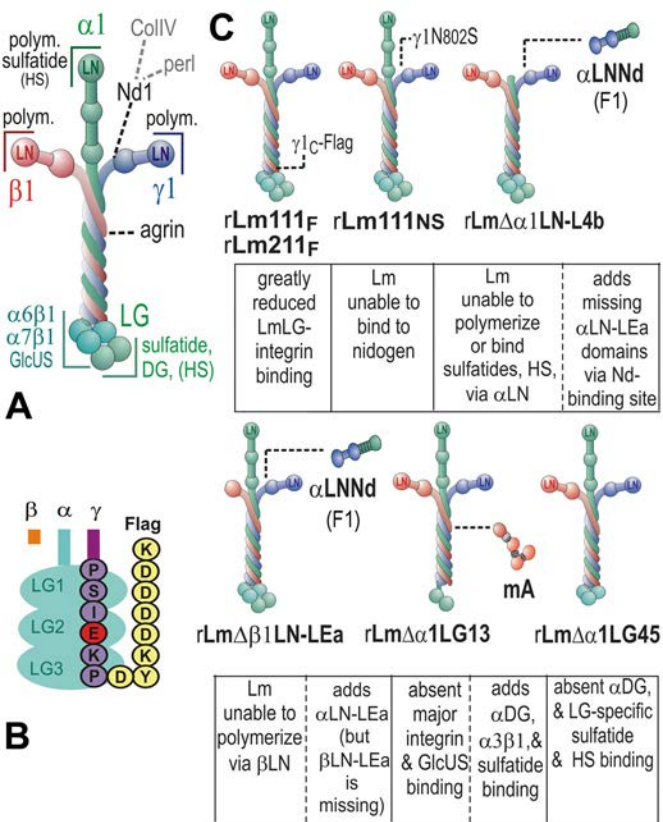


Fig. 4

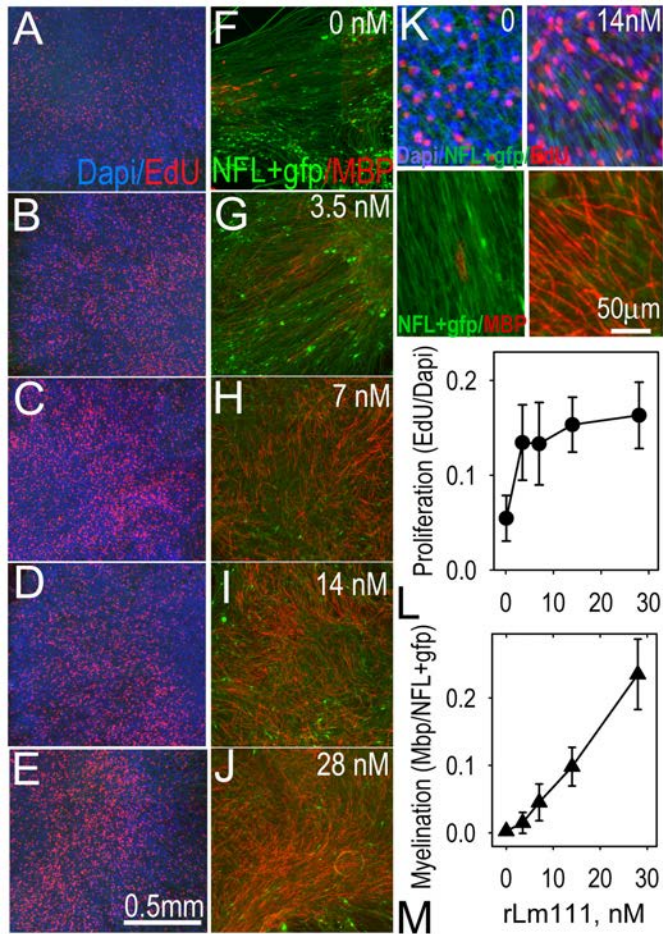


Fig. 5

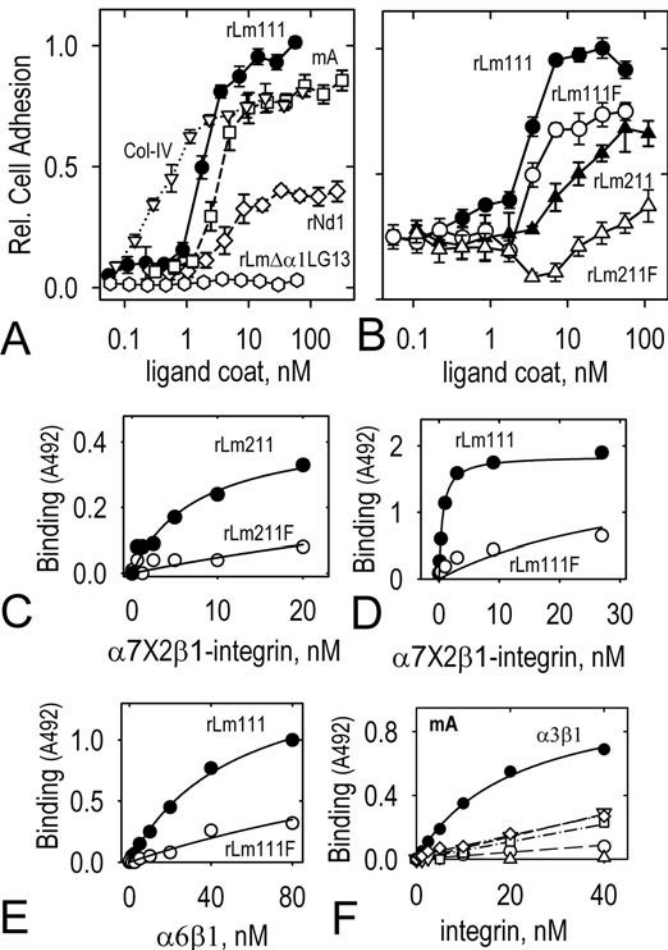
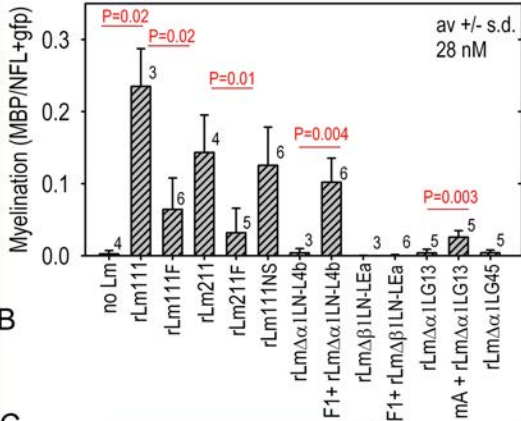
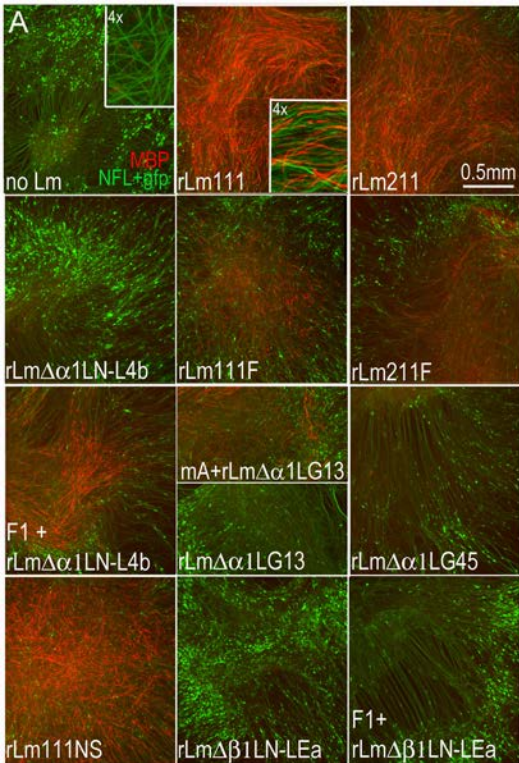
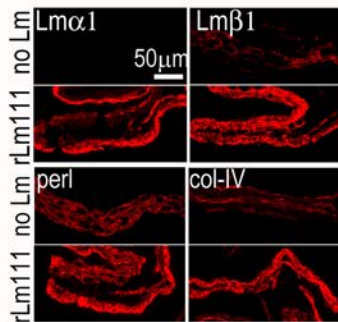


Fig. 6



B

C



D

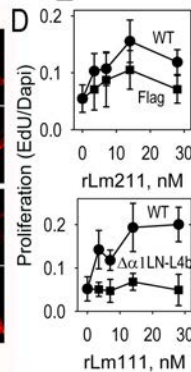


Fig. 7

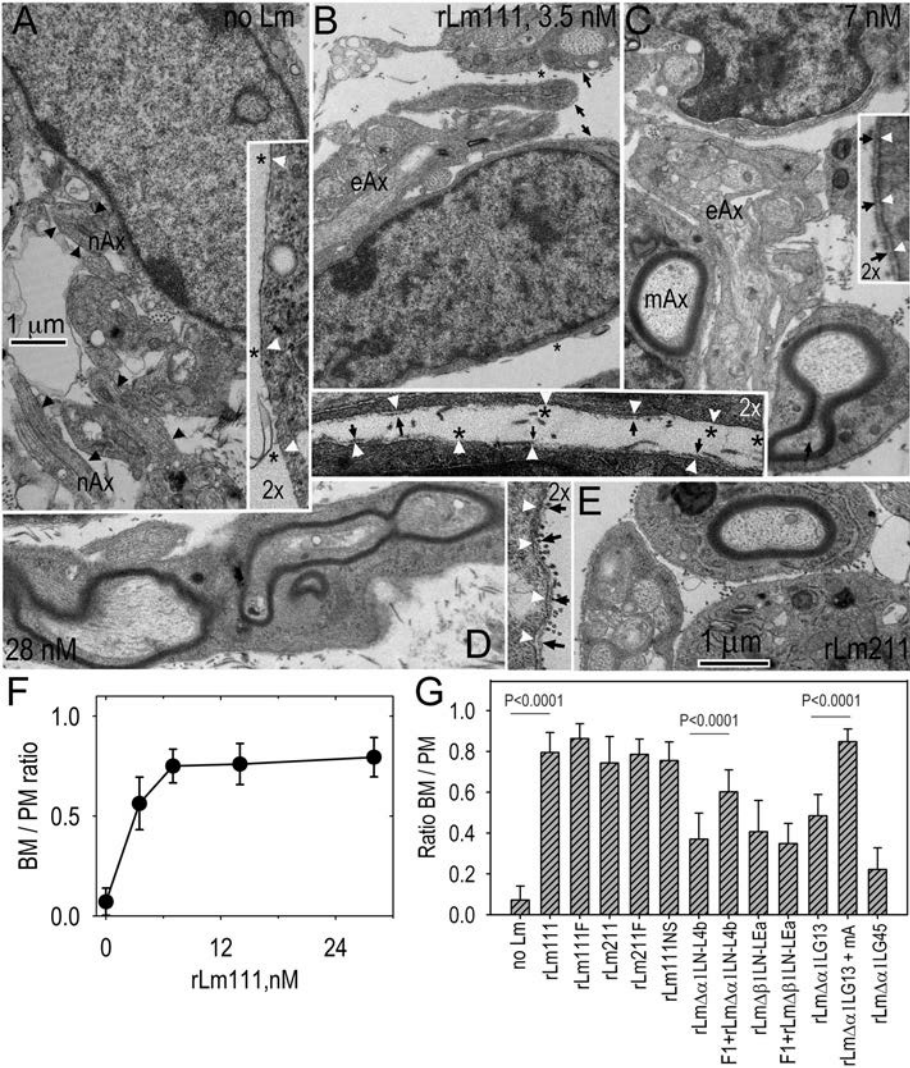


Fig. 8

SUPPLEMENTAL FIGURES

Figure S1. *Mouse expression of laminins and other subunits.* **A.** *Lmc1*^{fl^{neo}/fl^{neo}} mice were mated with FLP mice to excise the PGKneo cassette and then bred with +/- mice. The fl/- offspring did not have a gait abnormality and appeared normal. mRNA from the nerve and muscle of these mice was increased and similar to those of +/- mice. **B.** No compensatory changes in mRNA expression were noted for laminin $\alpha 2$, $\beta 1$, $\gamma 3$ and $\alpha 4$ from the indicated fl^{neo}/- tissues. Quadriceps skeletal muscle (**C**), lung (**D**), kidney (**E**) and colon (**F**) from fl^{neo}/+ and fl^{neo}/- mice were stained with the indicated laminin subunit, perlecan, collagen-IV, integrin and dystroglycan antibodies. Laminin $\gamma 1$, $\beta 1$, and $\alpha 2$, subunit immunostaining, along with that for collagen-IV (but not integrin or dystroglycan) was reduced in skeletal muscle. A slight decrease of Lm $\gamma 3$ was noted. Adult fl^{neo}/- lung showed only slight reduction of Lm $\beta 1$ and other subunits (not shown). Little change in laminin (shown Lm $\gamma 1$) was noted in kidney (with the exception of a small reduction in glomerulus) or in colon.

Figure S2. *Ultrastructural morphometry of adult sciatic nerve.* **A.** Measurements of fraction of sorted axons that were myelination (M), enveloped within Remak bundles (E), and as bundles of axons contained within a single myelinated SC (P, polyaxonal myelination) measured from micrographs at 2800 to 3000 magnification (average and S.D., three levels). Inset shows fraction of nuclei within SCs that do not myelinate (darker shading indicates sub-fraction of cells not adjacent to axons). Many SCs appear to fail to engage in myelination in fl^{neo}/- nerve. **B.** Frequency histogram of cross-sectional area ratio of axon/myelin+axon. Axons of *Lmc1* fl^{neo}/- nerves were hypomyelinated. **C.** Frequency histogram of cross-sectional areas of axons that were myelinated. The largest caliber axons found in fl^{neo}/+ nerves are not present in fl^{neo}/- nerves. This may reflect reduced axonal growth or even loss of axons. **D.** Frequency histogram of unmyelinated axons in fl^{neo}/+ (contained in enveloped Remak bundles) and fl^{neo}/- (naked or incompletely enveloped axons) sciatic nerve. The naked axons of fl^{neo}/- mice have the calibers including and exceeding those found in normal Remak bundles.

Figure S3. *Ultrastructure of postnatal day 5 nerve.* **Panels A-H:** Large-caliber myelinated axons and small axons during SC sorting are seen in fl^{neo}/+ in (A) and fl^{neo}/- sciatic nerve (B,C). Substantial groups of unsorted axons are seen in the latter. Basement membrane coverage of fl^{neo}/+ nerves is essentially continuous in both myelinated axons (MA) and SC lamellipodial processes (LP) adjacent to axons (D,F) while coverage of fl^{neo}/- nerves is discontinuous on SC

processes (D,G). Panels and 2-fold magnified insets indicate BM (arrows) and gaps (asterisks) present in $fl^{neo}/-$ nerves. D' shows polarized SC lamellipodial process with BM on one side and axons on the other. Panels F and G show patterns of BM on myelinated axons (green) and SC lamellipodia adjacent to axons (red) as used to estimate the degree of SC coverage by BMs (plotted in G, average and S.D. of three levels, 6-12 images, 5000-8000x, each). Reduced coverage, reflecting basement membrane discontinuities (arrows indicate basement membrane segments; asterisks indicate gaps), is seen selectively in the $fl^{neo}/-$ cell processes.

Figure S4. Embryonic and Perinatal Peripheral Nerve Immunostaining. Hindlimb nerve from E18.5, P1 and P5 were immunostained for Lm β 1, collagen-IV, and integrin- α 6 as shown (red) relative to neurofilament-200 (NFL, green). BM component immunofluorescence was reduced in $fl^{neo}/-$ nerve compared to $fl^{neo}/+$ nerve at all stages.

Figure S5. Skeletal muscle morphology. Panel A: H&E and trichrome staining of adult leg muscles. (a,b): vastus lateralis; (c,d): adductor longus. Individual $fl^{neo}/-$ muscle fibers were of smaller diameter, some with central nuclei (arrows), but otherwise normal in appearance. (e,f): No obvious increase in interstitial collagen between myofibers was appreciated. Panel B: Graph of the number of central nuclei showed an increase of centrally-nucleated myofibers ($P < 0.002$, $n=5$) in $fl^{neo}/-$ muscle. Panel C: Graph of quadriceps muscle fiber diameters reveals about a two-fold decrease ($P < 0.001$, $n = 5$) in $fl^{neo}/-$ mice. Panel D: Ultrastructure: The sarcolemmal basement membrane (arrowheads) of $fl/-$ quadriceps muscle was of normal appearance. However, a slight increase of adjacent interstitial collagen fibrils (seen as fibril cross-sections) was noted.

Figure S6. Dorsal root ganglia cultures. Panel A. Laminin α 2 immunostaining of adeno-cre virus laminin-inactivated DRG explants. DRGs were excised from E13.5 mouse $Lamc1^{fl^{neo}/fl^{neo}}$ embryos, adhered to collagen-coated tissue culture wells, and maintained in culture for four days. DRGs were then treated with adeno-cre-gfp virus (- day 4). Some of the DRGs were not treated with exogenous laminin and were harvested at the indicated times. Others were treated with rLm-211 (wild-type) at different concentrations starting from the time of virus addition and maintained at that concentration until harvesting. The culture medium was switched to ascorbate-containing "myelination" medium (at day 0) and the DRGs were cultured for an additional six days. DRGs were isolated at the indicated times, fixed, sectioned perpendicular to the tissue culture plane, and immuno-stained with antibody specific for the laminin α 2 subunit.

DRGs maintained without recombinant laminin exhibited little (well below that observed with 3.5 nM added laminin) or no laminin immunostaining at all time points. Treatment with rLm211 resulted in substantial immunostaining with increasing brightness detected with increasing laminin concentrations (day 6 myelination medium). **Panel B.** Concentration-dependency of myelination of DRGs treated with rLm111 measured as cumulative MBP-stained segment lengths/mm² of DRG (average and standard deviation, number of DRGs indicated next to each data point). The total length/DRG increased as a function of concentration with a decrease in slope at higher concentrations. **Panel C.** Plot of MBP-stained segment lengths (average and s.d.; total segment measurements indicated in red). **Panel D.** Plot of cumulative myelinated segment lengths per DRG area (average and s.d., number of DRGs and P values in red) for the indicated conditions. Loss of LG-domains that mediate adhesion and integrin-binding, selective loss of LG-integrin binding, and loss of polymerization all separately reduced myelinated segment density (similar relationships were observed with myelination measured by segmentation analysis (Fig. 7). Reductions in segment lengths were associated with low levels of myelination. **Panels E-H.** Electron micrographs of Schwann cell axonal sorting. *Lamc1-fl/fl* DRGs, inactivated with adeno-cre-gfp virus, were denied laminin (E, no laminin) or treated with 3.5 nM wild-type rLm111 (F), 28 nM non-polymerizing rLm $\Delta\alpha$ LN-L4b (G), or 28 nM wild-type rLm111 (H), all in the presence of 28 nM nidogen-1 and in the presence of ascorbate for six days. In the absence of added laminin, most axons were naked (N) and often grouped in large bundles (right side). While some of the axons were in direct contact with SCs, they were rarely surrounded by cell processes (when such processes were observed (inset), the processes were usually of short length resulting in incomplete bundling (B')). At low concentrations of laminin, many of the axons were noted to be partially (one-half to two-thirds) grouped into bundles by lamellipodia (B') or more fully grouped (B), and with a substantially increased fraction of axons sorted (S) within cells and cell processes, and located fully and individually within Schwann cells (1:1), with infrequent axonal myelination (M). At high concentration of laminin (H, two frames), naked axons were only occasionally encountered. In contrast, substantial fractions of sorted and 1:1 segregated axons were present. **Panel I.** Plots of the distribution of naked (N), bundled (B, includes B'), sorted (S) and myelinated (M) axons as described were determined by from multiple micrographs. The highest degree of sorting was detected following treatment with 28 nM laminin-111, in marked contrast to no treatment. Treatment with wild-type rLm211 considerable sorting; however, this was less-advanced compared to Lm111. The distribution of sorted axons was further reduced with Flag-tag modified rLm211. Laminin unable to polymerize (rLm $\Delta\alpha$ 1LN-L4b) or lacking LG4-5 cell-adhesion domains (rLm $\Delta\alpha$ 1LG4-5) had a considerable

fraction of naked axons; however, it exhibited prominent bundling and moderate fractions of sorted axons, unlike the no-treatment condition.

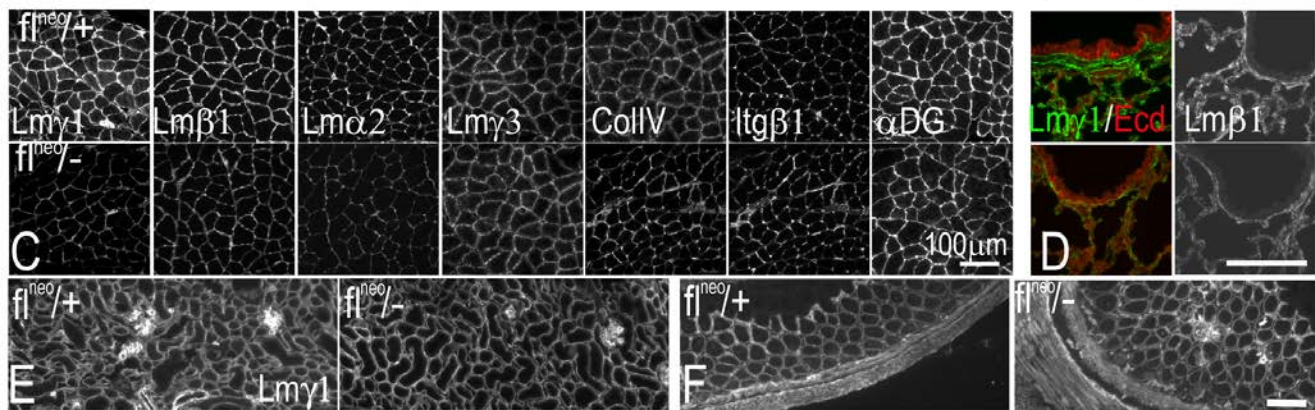
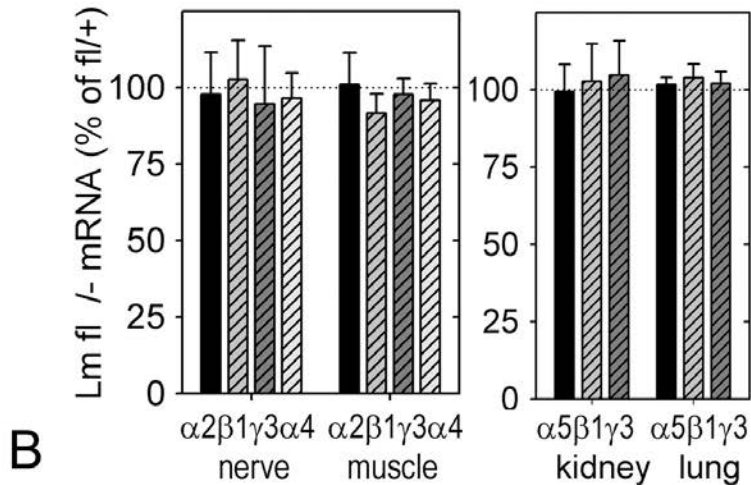
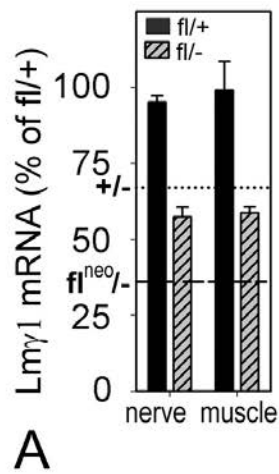


Fig. S1

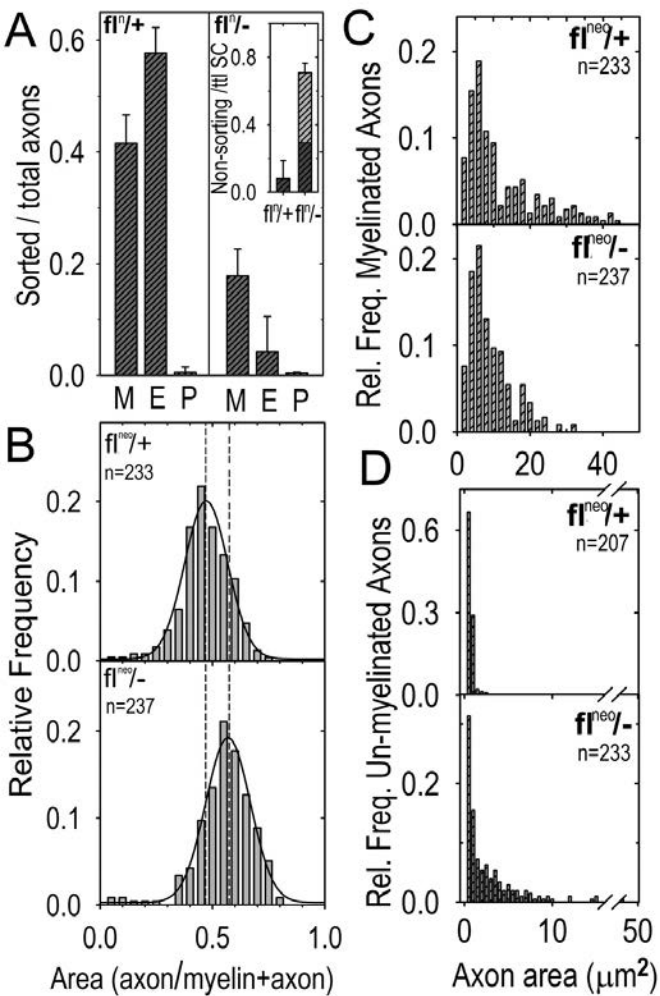


Fig. S2

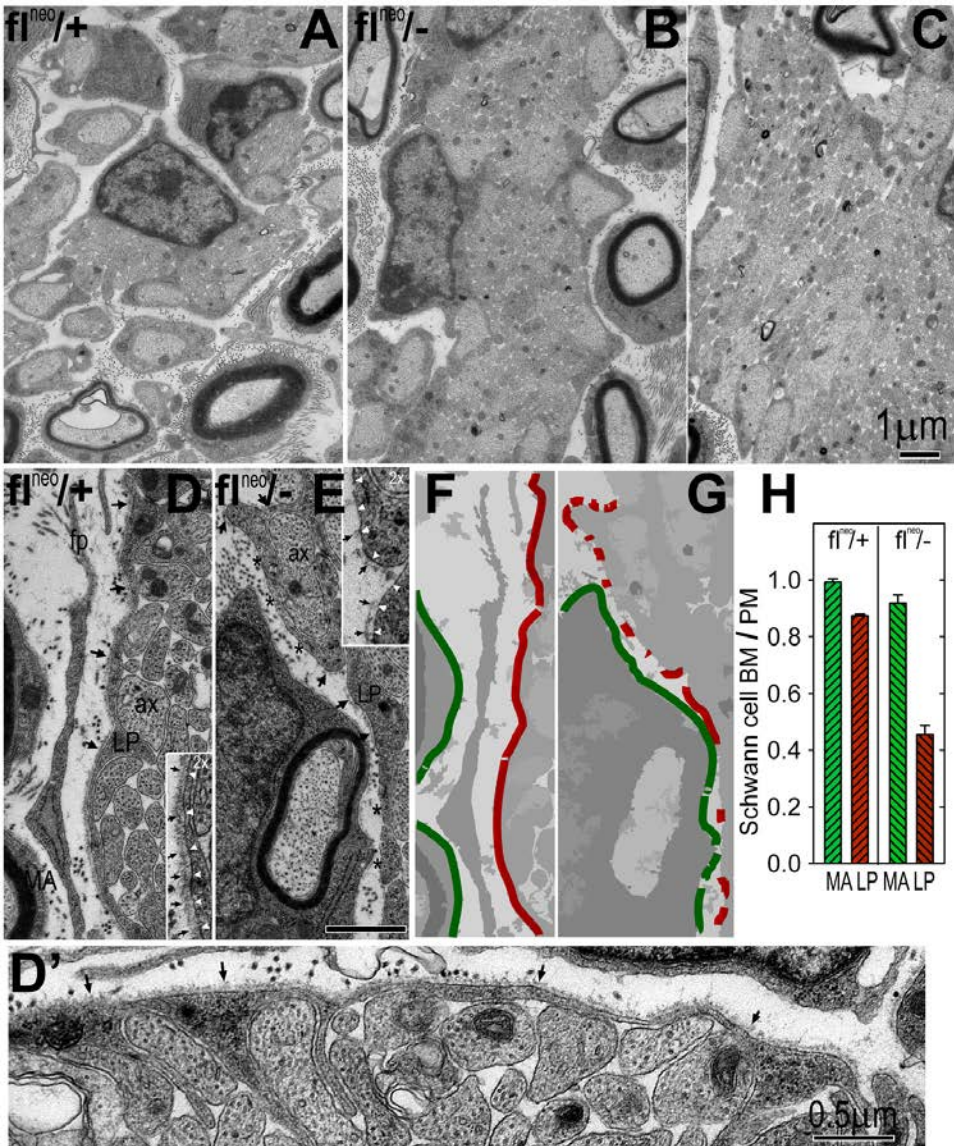


Fig. S3

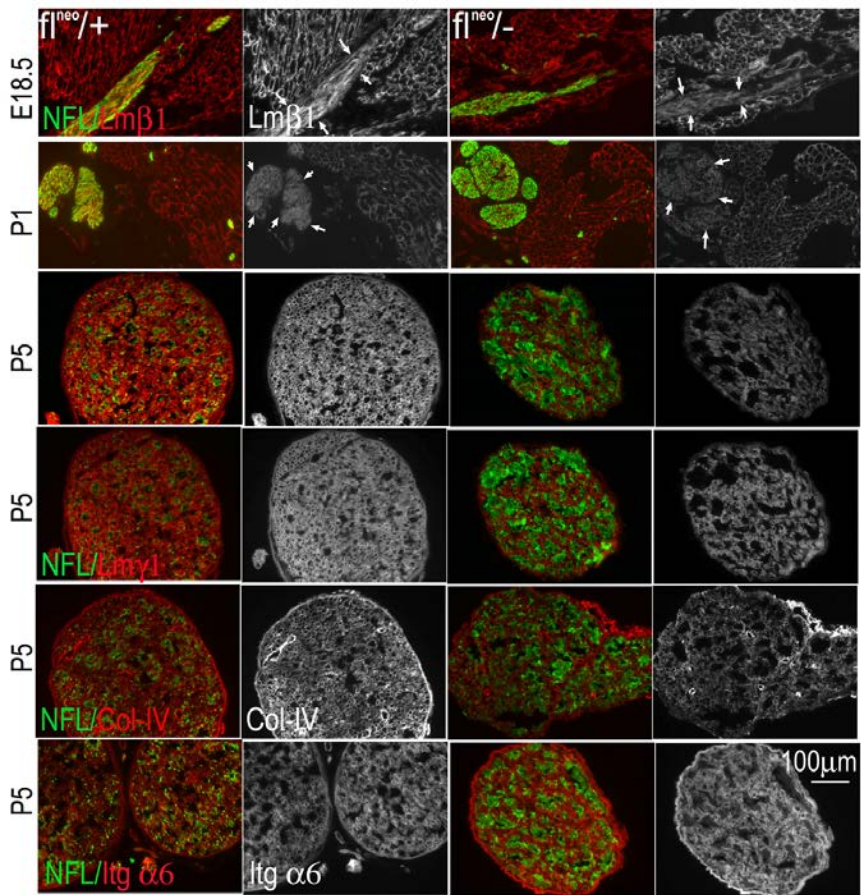


Fig. S4

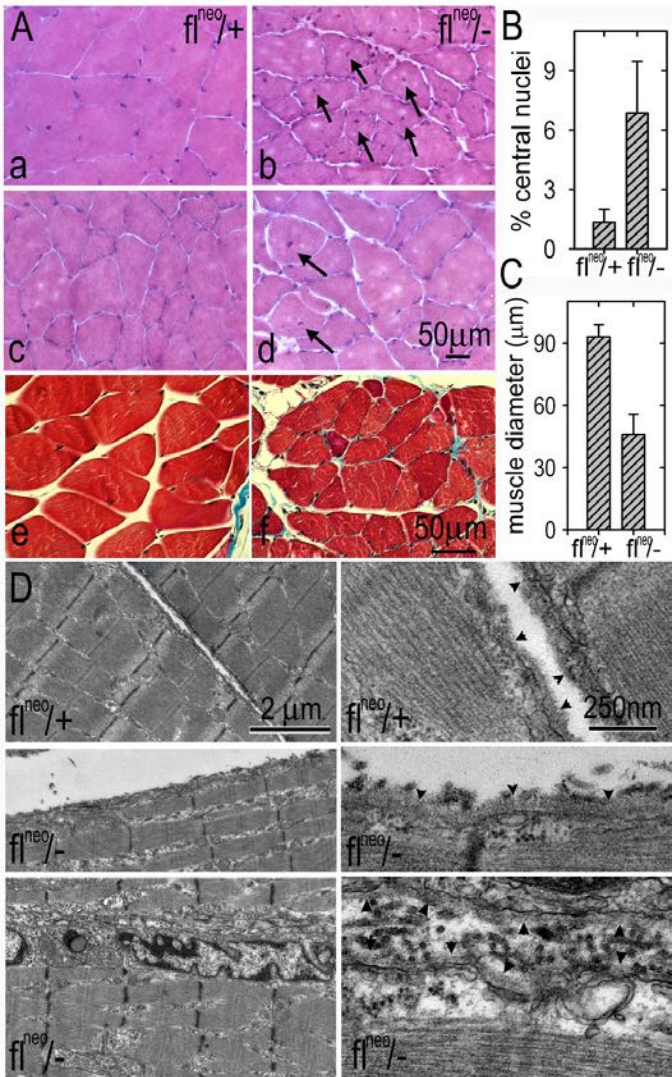


Fig. S5

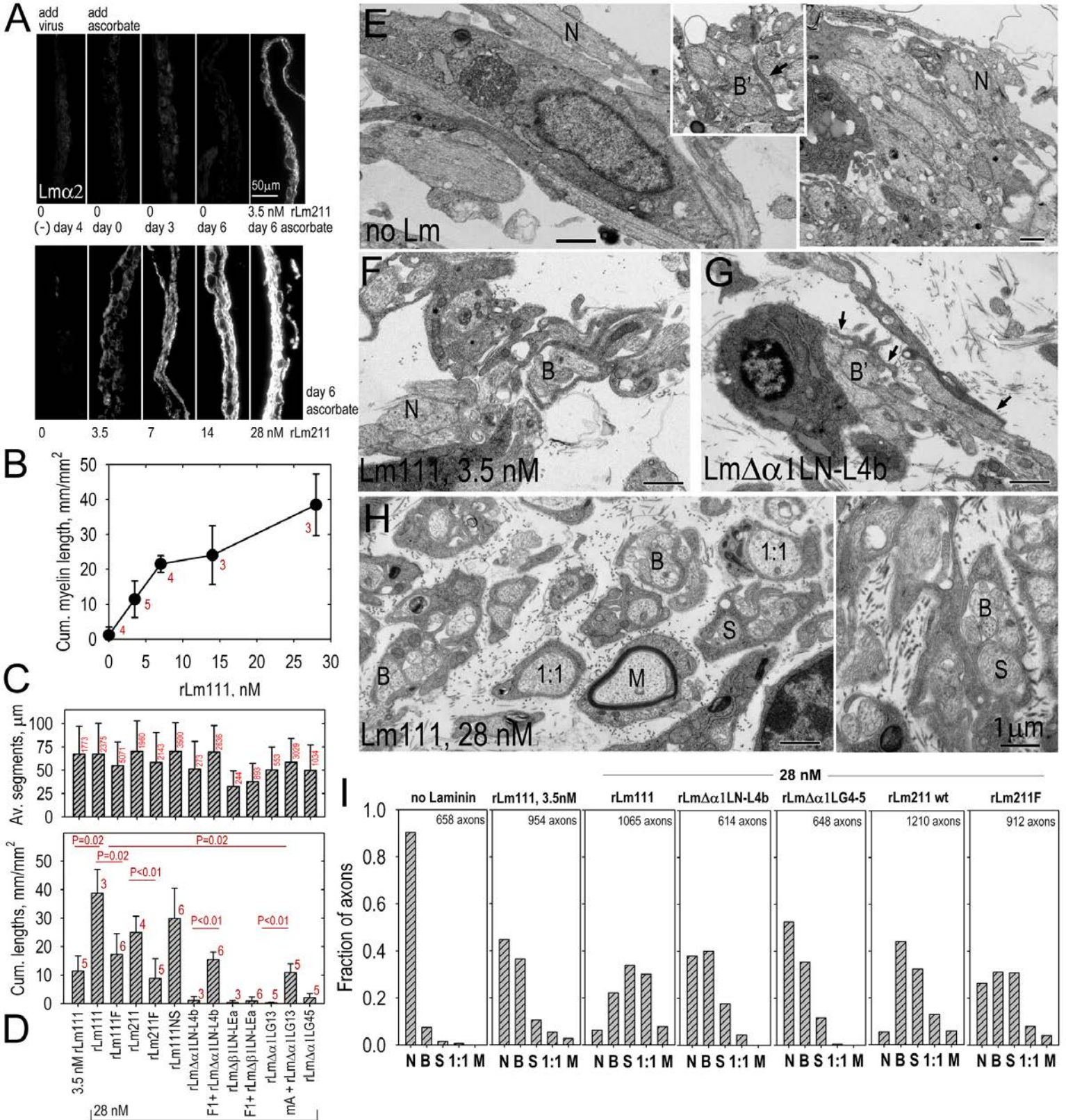


Fig. S6